Multi-omics comparisons of different forms of centronuclear myopathies and the effects of several therapeutic strategies

Sarah Djeddi, David Reiss, Alexia Menuet, Sébastien Freismuth, Juliana de Carvalho Neves, Sarah Djerroud, Xènia Massana Munoz, Anne-Sophie Sosson, Christine Kretz, Wolfgang Raffelsberger, et al.

Multi-omics comparisons of different forms of centronuclear myopathies and the effects of several therapeutic strategies

Sarah Djeddi[1], David Reiss[1], Alexia Menuet[1], Sébastien Freismuth[1], Juliana de Carvalho Neves[1], Sarah Djerroud[1], Xènia Massana-Muñoz[1], Anne-Sophie Sosson[1], Christine Kretz[1], Wolfgang Raffelsberger[1], Céline Keime[1], Olivier M. Dorchies[2], Julie Thompson[3], Jocelyn Laporte[1*]

[1]Institut de Génétique et de Biologie Moléculaire et Cellulaire (IGBMC), CNRS UMR7104, INSERM U1258, Université de Strasbourg, 67404 Illkirch, France

[2]Pharmaceutical Biochemistry, Institute of Pharmaceutical Sciences of Western Switzerland (ISPSO), University of Geneva, Geneva, Switzerland

[3]Complex Systems and Translational Bioinformatics (CSTB), ICube laboratory – CNRS, Fédération de Médecine Translationnelle de Strasbourg (FMTS), Université de Strasbourg, Strasbourg, France

*To whom correspondence may be addressed: Jocelyn Laporte; Email: jocelyn@igbmc.fr

ORCID:

Sarah Djeddi: 0000-0001-9446-6976

Xènia Massana-Muñoz 0000-0003-3652-9574

Olivier M. Dorchies: 0000-0002-6665-7887

Wolfgang Raffelsberger: 0000-0002-7426-3693

Jocelyn Laporte: 0000-0001-8256-5862

Abstract

Omics analyses are powerful methods to obtain an integrated view of complex biological processes, disease progression or therapy efficiency. However, few studies have compared different disease forms and different therapy strategies to define the common molecular signatures representing the most significant implicated pathways. Here, we used RNA sequencing and mass spectrometry data to profile the transcriptomes and proteomes of mouse models for three forms of centronuclear myopathies (CNM), untreated or treated with either a drug (tamoxifen), antisense oligonucleotides reducing the level of dynamin 2 (DNM2), or following modulation of dynamin 2 or amphiphysin 2 (BIN1) through genetic crosses. Unsupervised analysis and differential gene and protein expression were performed to retrieve CNM molecular signatures. Longitudinal studies before, at and after disease onset highlighted potential disease causes and consequences. Main pathways in the common CNM disease signature include muscle contraction, regeneration and inflammation. The common therapy signature revealed novel potential therapeutic targets including the calcium regulator sarcolipin. We identified several novel biomarkers validated in muscle and/or plasma through RNA quantification, western blotting and ELISA assays, including ANXA2 and IGFBP2. This study validates the concept of using multi-omics approaches to identify molecular signatures common to different disease forms and therapeutic strategies.

Keywords: genetic disease, congenital myopathy, centronuclear myopathy, myotubular myopathy, XLMTM, MTM1, myotubularin, omics, biomarker, myostatin, RNA interference

Background

In recent years, omics strategies (e.g. transcriptome, proteome etc.) have become powerful methods to obtain an unbiased and integrated view of complex biological processes, disease progression or therapy efficiency [1, 2]. Most previous studies focused on a single disease or therapeutic approach. However, omics have the potential to identify molecular signatures common to different disease forms or to several therapeutic strategies. Here, we performed omics analyses in mouse models faithfully mimicking different forms of centronuclear and myotubular myopathies treated or not with different therapeutic strategies to identify common disease and therapy signatures.

Centronuclear and myotubular myopathies (CNM) are a sub-group of congenital myopathies whose clinical signs develop around birth. They are rare genetic diseases appearing around birth and with a strong medical impact on patient survival and quality of life [3, 4]. CNM are characterized by generalized muscle weakness and hypotonia impairing breathing capacity [5]. Histological hallmarks of patients' muscle include the presence of internal or central nuclei that are normally at the fiber periphery, aggregation of oxidative staining, hypotrophy of myofibers that also present with a rounder shape, predominance of oxidative type I fiber, and structural disorganization of sarcomeres and triads [6]. Several genes were found mutated in different forms of CNM. The most common and severe form, X-linked CNM which is also called myotubular myopathy (MIM#310400), is due to loss-of-function mutations in *MTM1* coding for the lipid phosphatase myotubularin [7]. Dominant forms are linked to mutations in *DNM2* (MIM#160150) coding the large GTPase dynamin 2 implicated in membrane trafficking and fission [8]. Some *DNM2* mutations lead to a neonatal form, such as the Ser619Leu missense mutation, while others are associated with later onset [9, 10]. Recessive and dominant forms are also due to mutations in *BIN1* (MIM#255200), coding for the membrane curvature remodeling protein amphiphysin 2 [11, 12]. These three forms represent the main forms of CNM. Nevertheless, additional genes are implicated in phenotypes overlapping with CNM such as *RYR1*, *TTN*, *SPEG*, *CACNA1S* or *PYROXD1* [3, 13, 14]. *SPEG* is linked to CNM with cardiomyopathy, while the histopathology associated with the other genes combines internal nuclei with additional defects such as cores or protein inclusions.

Previous studies in cellular and animal models and in patients' muscle biopsies for the canonical CNM forms suggested several pathomechanisms in skeletal muscle, including defects in triad structure and deficient excitation-contraction coupling, altered organelle positioning and function, abnormal neuromuscular junction (NMJ), deficient satellite cells, and dysregulation of autophagy [4, 15-17].

Defects in the genes implicated in the three canonical CNM forms were modelled *in vivo* in different organisms, ranging from yeast, *C. elegans*, drosophila, zebrafish and mouse [17, 18]. In addition, spontaneous mutations in either *MTM1* or *BIN1* were found in dogs developing CNM [19-22]. In mice, the *Mtm1*$^{-/y}$ knockout mouse develops a progressive myopathy with a histopathology mimicking patient hallmarks [23]. Additional *Mtm1* knockout lines were generated and showed a similar phenotype, while the *Mtm1*$^{RC/y}$ knock-in led to a milder phenotype [24-26]. Concerning *Dnm2*, knock-in mice for the most common mutations in the mildest form (Arg465Trp ; *Dnm2*$^{RW/+}$) or the severe neonatal form (Ser619Leu ; *Dnm2*$^{SL/+}$) were generated and reproduce a mild or severe muscle weakness, respectively, with CNM-like histopathology without centralized nuclei [27, 28]. For *Bin1*, full loss of BIN1 in *Bin1*$^{-/-}$ mice is perinatally lethal, preventing the comparison with the other CNM models [29, 30]. We recently created a mouse model with a skeletal muscle specific *Bin1* deletion that is viable and faithfully reproduces the decreased muscle force and most histopathological hallmarks of CNM (*Bin1*$^{mck-/-}$; unpublished). Here, we focus on omics analysis of *Mtm1*$^{-/y}$, *Bin1*$^{mck-/-}$, *Dnm2*$^{SL/+}$ mice, since they represent faithful models for the three canonical CNM forms and the mice share a similar skeletal muscle organization with patients.

Several therapeutic proof-of-concepts were recently validated in different CNM models, including the three CNM mice investigated here [17]. Adeno-associated virus (AAV) transduction of MTM1 or its closer homolog MTMR2 rescued the *Mtm1*$^{-/y}$ mouse, and AAV-MTM1 was further validated in the MTM1 Labrador model and recently injected in patients in a clinical trial [31-33]. Downregulation of DNM2 level were found increased at least in *Mtm1*$^{-/y}$ mice and MTM1 patients, whereas normalization of DNM2

level rescued the *Mtm1*$^{-/y}$ mouse, the *Bin1*$^{-/-}$ and *Bin1*$^{mck-/-}$ mice, and both *Dnm2*$^{RW/+}$ and *Dnm2*$^{SL/+}$ mice [28, 34-36]. DNM2 was reduced through three methods : genetic cross with a *Dnm2*$^{+/-}$ mouse, shRNA, or antisense oligonucleotides [34, 37, 38]. Overexpression of BIN1 through genetic cross with a Tg*BIN1* mouse or AAV-*BIN1* expressing human *BIN1* rescued *Mtm1*$^{-/y}$ and *Bin1*$^{-/-}$ mice [39]. In addition, treatment with tamoxifen, an estrogen modulator already used in clinic for breast cancer, partially rescued the *Mtm1*$^{-/y}$ mouse, potentially representing a drug repurposing strategy [40, 41]. Additional potential therapies have been tested in mice and other CNM models, and include *Dnm2* allele-specific silencing or trans-splicing, *Pik3c2b* downregulation, mTOR or acetylcholine esterase inhibitors [17].

To identify the main pathomechanisms, potential biomarkers and novel therapeutic targets for different forms of CNM, we performed transcriptome and proteome analyses of muscles from *Mtm1*$^{-/y}$, *Bin1*$^{mck-/-}$ and *Dnm2*$^{SL/+}$ mice either developing the disease or treated with 3 different therapies including two methodological approaches for one of the targets. We identified disease and therapeutic molecular signatures common to the three main forms of CNM.

Results

Animal models, treatments and omics strategies

In mice, muscle embryonic development proceeds from E10.5 to birth that happens at about E19 [42]. Then, muscle growth during postnatal maturation follows 2 phases: one based on satellite cells fusion up to 2-3 weeks (w) and a second based on growth factor signaling from weaning (around 3 w of age) to adulthood at 7 w (Figure 1a) [43, 44]. *Mtm1*$^{-/y}$ mice develop a progressive myopathy from 2-3 w leading to a strong muscle hypotrophy and decreased locomotor activity, and death by about 8 w. *Bin1*$^{mck-/-}$ mice have near normal locomotor activity and decreased muscle force at 8 w. *Dnm2*$^{SL/+}$ mice have some feeding defects at birth correlating with decreased body weight, strong muscle atrophy and decreased locomotor activity, and survive in adulthood. All these mice have CNM-like histopathology by 7-8 w.

Based on the key steps of muscle maturation and on the disease progression in the different models, we performed RNAseq for transcriptome analysis in tibialis anterior (TA) muscle from the 3 CNM mice at 7 w. In addition, RNAseq was done at E18.5 and 2 w for a longitudinal follow-up of *Mtm1*$^{-/y}$ mice. Mass spectrometry for proteome analysis was performed in TA at E18.5, 2 w and 7 w for a longitudinal follow-up in *Mtm1*$^{-/y}$ mice (Table S1).

Several therapeutic approaches were applied to *Mtm1*$^{-/y}$ mice and consisted of either *BIN1* overexpression by crossing with Tg*BIN1* mice (*Mtm1*$^{-/y}$Tg*BIN1*), tamoxifen supplementation in food, or DNM2 downregulation by crossing with *Dnm2*$^{+/-}$ mice (*Mtm1*$^{-/y}$*Dnm2*$^{+/-}$)(Figure 1b; Table S1). DNM2 was also downregulated with another method, systemic injection of antisense oligonucleotides (ASO *Dnm2*), in *Bin1*$^{mck-/-}$ and *Dnm2*$^{SL/+}$ mice and compared to injection of PBS or control ASO. All these treated cohorts were analyzed by RNAseq in TA at 7 w and compared to the above untreated mice. In addition, RNAseq and mass spectrometry of TA from *Mtm1*$^{-/y}$*Dnm2*$^{+/-}$ mice was performed at E18.5, 2 w and 7 w. Muscle samples were obtained from our previous studies reporting therapeutic efficacy [28, 34, 39, 40].

In addition, in order to identify dysregulated muscle proteins that are potentially circulating, mass spectrometry was performed *in sera* from WT mice at 7 w and compared with the above muscle transcriptome and proteome data.

Influence of the genetic and environment backgrounds

To assess the impact of the genetic background and animal housing on the transcriptome, we analyzed different RNAseq data from different cohorts of the same *Mtm1*$^{-/y}$ mouse line on different genetic backgrounds and raised in different animal houses. Four different cohorts were evaluated (Table 1): cohort MTM1-a was crossed on the 129Pas background and bred in France, cohort MTM1-b was on a 50% 129Pas and 50% C57BL/6N background and raised in the same animal facility in France, cohort

147 MTM1-c was raised in Switzerland on the 129Pas background, and cohort MTM1-d was bred in Canada
148 on a C57BL/6J background. Muscles used for transcriptomics for the first three cohorts were TA analyzed
149 at 7 w. The transcriptome for cohort MTM1-d was previously published and done from quadriceps at 5
150 w [41]. We compared differentially expressed genes between *Mtm1*$^{-/y}$ and WT mice for the different
151 cohorts. The threshold used to define dysregulated genes was set at Log2FC+/-1 and p-value < 0.05. The
152 number of dysregulated genes in *Mtm1*$^{-/y}$ mice ranged from 1275 to 1981 (Figure 2a). A total of 287
153 genes were found commonly dysregulated across the different cohorts. These genes correspond to the
154 disease signature following MTM1 loss, and their expression is not impacted by any environmental or
155 housing parameters, the genetic background, or the muscle analyzed (Table S2). As expected, the most
156 divergent transcriptome was from cohort 4 that differs from the other cohorts by both the genetic
157 background and the muscle, as 56% of dysregulated genes are specific to this cohort versus 23 to 33%
158 for the other cohorts.
159 All the common dysregulated genes followed the same trend in the different cohorts. We found 67
160 common genes were downregulated and 220 common genes upregulated. Gene ontology (GO) analysis
161 revealed an enrichment for muscle development and contraction, cell adhesion and immune cells (Figure
162 2b). The most upregulated protein coding genes were *Sox11*, *Krt18*, *Mt3*, *Msln*, *Hsf2bp* and *Fosl1*, and
163 the most downregulated were *Mstn*, *Cdh4*, *Edn3*, *Mtm1*, *Ighm*, *Fam19a4*, *Nt5c1a* and *Amd1* (Table 2).
164 We thus report the disease signature for MTM1-CNM that is independent of the genetic and
165 environmental backgrounds in mice.
166
167 **Conserved disease signatures linked to *MTM1* mutations among species**
168 We next explored the conservation of the disease signature linked to MTM1 loss in different species. In
169 human (Biceps brachii or quadriceps), Noguchi et al. performed microarray analysis on a set of 4200
170 genes previously known to be expressed in skeletal muscle from 8 patients with different *MTM1*

mutations [45]. 183 genes were significantly dysregulated compared to unaffected individuals. Of note, *MTM1* was not reported dysregulated in this study. In dog, Dupont et al. used RNAseq to analyze two hindlimb muscles from Labradors lacking MTM1 [46]. They found 824 and 1122 genes differentially expressed in the Biceps femoris and the Vastus lateralis respectively, with 400 genes dysregulated in both muscles. Here, we used the 632 genes that we identified in the RNAseq analyses conducted in *Mtm1*$^{-/y}$ mouse cohorts MTM1-a, MTM1-b and MTM1-c at 7 w (Figure 2a and Table S3).

Interspecies analysis revealed 5 differentially expressed genes shared by mouse, dog and human (Figure 2c). Among them, *CHRND* and *CHRNA1* coding for two subunits of the acetylcholine receptor in the NMJ were upregulated (Figure 2d). *MYOG* (myogenin), coding for a transcription factor key in muscle differentiation was upregulated in dog and mouse and downregulated in human. *POPDC3* was upregulated in human and mouse and downregulated in dog, is also implicated in muscle development, and was found mutated in limb-girdle muscular dystrophy [47]. The majority of the dysregulated genes were specific to each species, therefore we analyzed them by GO enrichment and it revealed a few processes that might be species dependent, as hemostasis dysregulation in human or specific impact on kinase pathways in dog (Figure S1 and Table S4).

As the human data was based on microarray analysis of only a subset of genes, additional comparisons were done between dogs and mice and identified 63 additional genes dysregulated (Vastus Lateralis vs Tibialis anterior) (Figure 2c and Table S5), or 49 genes (Biceps Femoris vs Tibialis anterior)(Figure S1; Table S6). GO terms related to these genes were highly enriched in muscle development (Figure 2e). Among these genes, *Chrna1*, *Chrnd* and *Chrng* highlight the NMJ, and *Myog* and *Pax7* the transcriptional regulation of muscle differentiation and regeneration. Other examples confirmed by RT-qPCR included downregulation of *Mstn* (myostatin), a ligand of TGFβ receptor involved in muscle growth, and upregulation of *Fst* (follistatin), coding for an inhibitor of myostatin (Figure 2f). We found upregulation of *Igfbp2*, coding an insulin-like growth factor-binding protein potentially involved in

muscle differentiation and hypertrophy. *Cilp* was upregulated and codes for a regulator of IGF1 (insulin-like growth factor type 1) and TGFβ signaling. Genes coding for potential regulators of the Rac1-actin pathway, *Tiam2* and *Arhgap36*, were also upregulated.

Overall, defects in muscle development and the NMJ appear conserved in mouse, dog and human with MTM1-CNM. The more detailed investigations in mouse and dog highlighted additional pathways of interest such as muscle growth and repair.

Longitudinal molecular profiling of *Mtm1*$^{-/y}$ mice through disease progression

Several pathways were identified in the MTM1-CNM disease signatures at an age when mice, dogs and patients are strongly affected. To define the primary molecular causes versus consequences of the disease, we performed longitudinal analyses of the transcriptome and proteome of TA muscles from *Mtm1*$^{-/y}$ mice at pre-symptomatic age (E18.5), early (2 w) and late (7 w) disease stages (Figure 1a). We used the cohort MTM1-a, including untreated *Mtm1*$^{-/y}$ mice, *Mtm1*$^{-/y}$ mice rescued by *Dnm2* genetic downregulation, treated and healthy *Mtm1*$^{-/y}$*Dnm2*$^{+/-}$ mice, and their WT littermates (Table S1).

Principal component analysis (PCA) on transcriptome data showed that age explains most of the variance between the mouse groups as underlined by the first principal component (PC1 58%, PC2 13%, PC3 5% variance; Figure 3a and Figure S2). Separation of the genotypes appeared at PC4 (4% variance). Interestingly, this separation appeared at 2 w and increased at 7 w. No genes were significantly dysregulated at E18.5, indicating no difference between genotypes at late embryonic stage. A total of 1175 genes were dysregulated at 2 w and 1981 at 7 w (Figure 3b and Table S7). Potential disease causes found at 2 w are defects of muscle contraction, sarcomere organization and cell adhesion (GO term analysis; Figure 3b; Figure S3). Disease consequences found only at 7 w highlighted activation of the inflammation pathway, suggesting infiltration of affected muscles by immune cells. Volcano plots display the most dysregulated genes at 2 and 7 w (Figure 3c,d). As examples, the three most upregulated genes at both ages were *Sln* (sarcolipin), *Krt8* and *Krt18* (keratins)(Figure 3c-d). Dysregulation of these and

219 other genes was confirmed by RT-qPCR (Figure S4, S5). The downregulation of *Mstn*, observed in late
220 disease stage in dogs and mice, was already apparent at the 2 w early stage in mice (Figure 3e). An
221 example for sarcomere organization is *Ahnak2*, whose protein product (AHNAK 2) localizes to Z-line.
222 *Tnnt2* (cardiac troponin) and *Myl4* (cardiac myosin light chain) are implicated in muscle contraction,
223 expressed in embryonic but not adult skeletal muscle and in adult cardiac muscle under normal
224 conditions, and found upregulated in this myopathy. The cell adhesion was represented for example by
225 Itga3 (integrin). Genes underlying the activation of the inflammation pathway at 7 w include *Cxcl1*
226 (chemokine) and *Tlr2* (Toll-like receptor).
227 In parallel, PCA was also performed on proteome data and showed that the variance between the mouse
228 groups is first explained by age (PC1; 39% variance; Figure 4a) followed by genotypes (PC2; 7%).
229 Similarly to the transcriptome data, the genotype separation appeared at 2 w and increased at 7 w,
230 indicating no difference at E18.5. Out of 1462 proteins consistently detected in each of the muscle
231 samples, 168 proteins were dysregulated at 2 w and 496 at 7 w in the *Mtm1*$^{-/y}$ mice compared to WT
232 (Figure 4b and Table S8). Potential disease causes found at 2 w were related mainly to muscle sarcomere
233 and contraction (GO terms analysis; Figure S6). At 7 w, defects of muscle contraction pathway were
234 persistent, and at this late disease stage dysregulation of ribosomal biogenesis (translation) appeared. The
235 transcriptome and proteome data analysis consistently highlighted muscle contraction defects as a main
236 early sign of the disease. The late dysregulation of ribosomal biogenesis may reflect a compensatory
237 mechanism following alteration of protein homeostasis correlated with the strong fiber hypotrophy in
238 MTM1-CNM. Examples of dysregulated proteins implicated in muscle contraction include MYH2
239 (myosin heavy chain) mutated in a proximal myopathy with ophtalmoplegia (MIM#605337), and
240 TNNC1 (troponin) mutated in dilated cardiomyopathy (MIM#611879)(Figure 4c-e). These proteins
241 strongly correlate pathways and gene families found through the above transcriptome analysis: MYH2
242 and MYL4 are myosin heavy and light chains, respectively and TNNT2 and TNNC1 are troponins. All
243 four proteins are implicated in muscle contraction. Pearson correlation analysis did not underline a high

correlation between specific genes and proteins at 2 and 7 w (Figure S7), as generally reported in the literature [48]. In conclusion, while the same dysregulated genes/proteins are not necessarily highlighted by the transcriptome and proteome analyses, the same pathways and functions are consistently defective in early and late disease stages. Dysregulation in muscle contraction appears to be an early defect in the MTM1-CNM pathology in mice.

Disease signature common to several CNM forms

Next, we explored whether a common disease signature can unify the different CNM forms linked to either *MTM1*, *BIN1* or *DNM2* mutations. First, we compared the levels of these genes/proteins in the different corresponding models: the *Mtm1*$^{-/y}$, *Bin1*$^{mck-/-}$ and *Dnm2*$^{SL/+}$ mice (Table 3 and Figure S8). Apart from the lack of MTM1 and BIN1 proteins in their respective knockout mice, DNM2 was found slightly elevated (2.2 fold; p=0.057; [28]) in the *Dnm2*$^{SL/+}$ mouse. No strong alteration of the level of their RNA was detected in the corresponding RNAseq data. A slight increase in both BIN1 and DNM2 proteins was found in the *Mtm1*$^{-/y}$ mice, and DNM2 protein was slightly increased in *Bin1*$^{mck-/-}$.

Then, dysregulated genes were extracted from each individual cohort at 7 w: cohorts MTM1-a, MTM1-b, MTM1-c, cohort BIN1 (*Bin1*$^{mck-/-}$) and cohort DNM2 (*Dnm2*$^{SL/+}$), and compared to their respective WT littermates. For each cohort, disease models were well separated from the WT controls on the principal component 1 of the PCA (Figures 3a, 5a; Figure S9). The number of dysregulated genes correlated with the severity of the related models at this age: more than 1200 genes for the most severe *Mtm1*$^{-/y}$ mouse that does not survive beyond 9 w, 780 genes for the *Dnm2*$^{SL/+}$ mouse with strong locomotor deficiency, and 308 for the *Bin1*$^{mck-/-}$ mouse with a conserved locomotor function. Among the 25494 genes detected in all the different transcriptomes, 155 common dysregulated genes were identified (Figure 5b and Tables S7, S9, S10, S11, S12, S13). The main cellular component GO terms highlighted the NMJ, basement membrane, sarcomere and activation of the inflammation pathway, previously

identified as the main pathways dysregulated in the *Mtm1*$^{-/y}$ cohorts (Figure 5c). Thus, the main disease signature common to the three CNM models underlines defects in sarcomere maturation and function, and in NMJ maturation as main causes of muscle weakness, and alteration in cell adhesion and basement membrane as a potential explanation for the altered fiber shape. As previously noted for the *Mtm1*$^{-/y}$ cohorts, a potential increase in the inflammation transcriptome supports the infiltration of immune cells in the different models. Several genes associated with inflammation were shared between the different CNM forms as indicated by GO terms linked with macrophages (Figure 5c). Since inflammation was not previously demonstrated in CNM models, we labelled macrophages with an anti-CD68 antibody on TA muscle sections. We found a significant increase in macrophage infiltration in the 3 CNM mouse models (Figure 5 d,e).

RT-qPCR analyses confirmed the dysregulation of all the 14 genes tested in the three different mouse models (Figures S10, S11, S12). In particular, the common CNM disease signature encompassed genes coding for myosin (MYL4) and troponin (TNNT2) for sarcomere organization and contraction, acetylcholine receptor subunits (CHRNA1, CHRNA9, CHRND), the SOX11 and MYOG transcription factors, the calcium regulator sarcolipin (SLN), myostatin and follistatin, and several proteins further studied below (ANXA2, S100A4, CILP, FETUB, SERPINB1A, IGFBP2)(Figure 5f). Genes specifically dysregulated in each CNM forms have been analyzed by GO enrichment and revealed some specific features as hemostasis defect in the BIN1 cohort, or cardiac and lipid metabolism for the DNM2 cohort, which remain to be further explored (Figure S13 and Table S14).

It is interesting to note that orthologs of several genes in the common disease signature were previously associated with neuromuscular diseases: *LMNA* in Emery-Dreifuss muscular dystrophy and *KLHL40* in nemaline myopathy, *CHRNA1* and *CHRNAD* for myasthenic syndrome, *HSPB1* and *PDK3* for Charcot-Marie-Tooth peripheral neuropathy. Overall, the main defective pathways found in the MTM1-CNM

291 models are also altered in the BIN1-CNM and DNM2-CNM models, revealing the existence of a
292 pathomechanism common to most CNM forms.

293 **Therapy signature common to several rescuing approaches for different CNM forms**

294 The transcriptome responses to different treatments of these three CNM mouse models was assessed in
295 TA muscle at 7 w. *Mtm1*$^{-/y}$ mice were treated with the drug tamoxifen (cohort MTM1-c), or following
296 genetic crosses with mice either overexpressing human BIN1 (cohort MTM1-b; *Mtm1*$^{-/y}$Tg*BIN1*) or with
297 *Dnm2* downregulation (cohort MTM1-a; *Mtm1*$^{-/y}$*Dnm2*$^{+/-}$)(Figure 1b). A different methodology to reduce
298 DNM2, systemic injection of ASO *Dnm2*, was used to treat *Bin1*$^{mck-/-}$ (cohort BIN1) and *Dnm2*$^{SL/+}$ (cohort
299 DNM2) mice. All these therapies improved the phenotypes of the different disease models ([28, 34, 39, 40] and
300 unpublished for *Bin1*$^{mck-/-}$). In each cohort, 4 groups were studied: treated (=rescued) and untreated CNM
301 disease models and treated and untreated WT controls.

302 PCA showed that untreated and treated WT controls cluster together, suggesting treatments had no
303 general effects on WT mice (Figures 6a,3a and Figure S9). For example, only 112 genes were
304 dysregulated in tamoxifen-treated WT mice, while *Dnm2* was indeed found downregulated together with
305 15 other genes in WT treated with ASO *Dnm2* (Table S12). The transcriptome of tamoxifen treated
306 *Mtm1*$^{-/y}$ mice was similar to that of diseased *Mtm1*$^{-/y}$ mice, suggesting that tamoxifen did not have a
307 strong transcriptional effect. Genetic downregulation of *Dnm2* in *Mtm1*$^{-/y}$*Dnm2*$^{+/-}$ led to a partial rescue
308 of the transcriptome of *Mtm1*$^{-/y}$ mice. Analyzing in *Mtm1*$^{-/y}$*Dnm2*$^{+/-}$ mice over time, we found a partial
309 rescue of 255 genes over 1175 genes dysregulated in *Mtm1*$^{-/y}$ mice at 2 w, and 725 genes over 1981
310 dysregulated genes at 7 w disease stage (Figure 6b and Table S7). *Myh3*, *Myh8* and *Sln* are among the
311 best normalized genes at 2 w. Acute downregulation of *Dnm2* with ASO *Dnm2* in both *Bin1*$^{mck-/-}$ and
312 *Dnm2*$^{SL/+}$ mice also partially rescued their transcriptomes (Figure 6a). Genetic overexpression of *BIN1*
313 in *Mtm1*$^{-/y}$Tg*BIN1* normalized the transcriptome to a WT level. As a metric to compare the molecular
314 efficacy of the different therapies, we calculated the ratio of the number of genes dysregulated in the

315 rescued group versus the disease group over the number of genes dysregulated in the disease group versus
316 the WT control; in other words, the ratio of the therapy signature over the disease signature. The
317 percentage of rescued genes was 0.5% for the MTM1-c cohort (tamoxifen), 36% for the MTM1-a cohort,
318 43% for the DNM2 cohort and 47% for the BIN1 cohort (Dnm2 downregulation), and 96% for the
319 MTM1-b cohort (BIN1 overexpression; 1680 genes on 1745). Overall, BIN1 overexpression appears to
320 be the most efficient therapy to normalize the transcriptome defects of CNM in mice.
321 To determine the common therapy signature, we compared the transcriptome of the rescued mice versus
322 the transcriptome of the diseased mice for all cohorts except the MTM1-c cohort as tamoxifen treatment
323 had no strong transcriptomic impact. We found 42 genes defining the therapy signature common to all
324 therapies in all CNM forms and that were retrieved in the disease signature for most of them (Figure 6b
325 and Tables S9, S15). Comparison of the rescued versus WT transcriptomes identified no genes in
326 common that were resistant to all different therapies tested. The expression levels of several of these 42
327 genes was confirmed by RT-qPCR (Figure 6c and Figures S4, S5, S10, S11, S12). Depending on the
328 cohorts, expression of these genes was partially or fully rescued upon treatment. For example, *Anxa2*
329 expression was not rescued in the MTM1-a cohort (*Mtm1*$^{-/y}$*Dnm2*$^{+/-}$), while *Cilp*, *Fetub* and *Igfbp2* were
330 all dysregulated in the different diseased models and their expression rescued to WT level following any
331 treatments.
332 The proteins corresponding to these 42 genes of the common therapy signature could represent novel
333 therapeutic targets. To help pre-selecting the best candidates, we retrieved the 35 corresponding human
334 orthologs and interrogated a drug database (http://drugcentral.org)(Figure 6d). Two proteins (SCN5A,
335 SBK3) appeared directly targeted by several drugs, like the antiarrhythmic quinidine for the SCN5A
336 sodium channel, or nintedanib, an inhibitor of SBK3 and tyrosine kinases used for pulmonary fibrosis
337 and cancer. Other therapeutic targets that were dysregulated in a majority of cohorts include myosins,

troponins, myostatin or acetylcholine receptor subunits, for which *in vivo* modulation methods were already validated for other diseases.

Taken together, comparison of the three CNM models and several therapies underlined a common disease signature and a common therapy signature indicating potential therapeutic targets and biomarkers to follow disease severity or progression and therapy efficacy.

Identification of muscle and circulating biomarkers correlating with disease and therapy

To identify potential circulating biomarkers of disease state and therapy efficacy, we compared the list of genes in the disease signature and the therapy signature with proteins detected by mass spectrometry on the serum of WT mice at 8 w (Table S16), with public databases listing proteins detected in different fluids in human and mouse (GTEx, BioGPS, Illumina, GXD), and with the literature (Figure 7a). The following proteins were selected: ANXA2, CILP, FETUB, IGFBP2 and MSTN. To identify the best biomarkers, they were further screened by RT-qPCR, western blotting and ELISA in muscle and in plasma. The levels of all these RNAs were altered in the disease state and responded to the therapies in the 3 CNM mouse models, as validated by RT-qPCR in muscle (Figure 6c; Figures S4, S5, S10, S11, S12). ANXA2, FETUB and CILP proteins were found dysregulated in muscle from some or all CNM models by western blot (Figure 7b and Figure S14). For example, *Anxa2* (ANXA2) was significantly upregulated in muscles from 7 w old *Mtm1*$^{-/y}$, *Bin1*$^{mck-/-}$ and *Dnm2*$^{SL/+}$ mice at both RNA and protein levels, and its RNA was found already upregulated, albeit to a lesser extent, at 2 w in *Mtm1*$^{-/y}$ mice (2 fold at 2 w and 2.46 fold at 7 w).

Concerning circulating biomarkers, ELISA assays confirmed the presence of ANXA2, CILP, IGFBP2 and MSTN in the plasma from WT mice, as previously detected in serum by mass spectrometry (Figure 7c). Unlike in muscle, CILP levels in plasma were not changed in any CNM mouse models. Interestingly, the plasma level of IGFBP2 was significantly increased in *Mtm1*$^{-/y}$ mice. The alteration of *Igfbp2* RNA

362 levels in the *Mtm1*$^{-/y}$ muscle increased with age and disease progression, from 6 fold at 2 w (early disease
363 stage) to 17 fold at 7 w (late disease stage). To assess if circulating IGFBP2 is a biomarker common to
364 several CNM forms, ELISA assays were performed in *Bin1*$^{mck-/-}$ and *Dnm2*$^{SL/+}$ plasma at 7 w. The level
365 of IGFBP2 was changed only in *Mtm1*$^{-/y}$ mice, suggesting it could be a biomarker specific to the MTM1-
366 CNM form. Similarly, dysregulation of plasma protein content of ANXA2 and MSTN was revealed by
367 ELISA, specifically for the BIN1-CNM or MTM1-CNM models respectively. In both cases, these
368 biomarkers responded to the therapies. The increase in ANXA2 plasma protein content in *Bin1*$^{mck-/-}$ mice
369 was normalized upon DNM2 decrease with ASO *Dnm2*. The strong decrease in MSTN plasma protein
370 content in *Mtm1*$^{-/y}$ mice was normalized upon BIN1 overexpression.
371 Overall this screening strategy, from RNAseq based discovery, to RT-qPCR and western blot in muscle,
372 and to ELISA in plasma, discovered ANXA2 as a muscle biomarker for several CNM forms and CILP
373 and FETUB for specific CNM forms. IGFBP2, ANXA2 and MSTN were found as circulating biomarkers
374 for specific CNM forms, and ANXA2 and MSTN plasma levels responded to the therapies.
375

376 **Discussion**

377 We performed a multi-omics meta-analysis of centronuclear myopathies through the comparison of
378 mouse models for the three main CNM forms and the comparison of three therapies with different targets.
379 We identified disease signatures for MTM1-CNM conserved in different genetic and environmental
380 backgrounds and in different species (mouse, dog, human). Longitudinal transcriptome and proteome
381 analysis of *Mtm1*$^{-/y}$ mice suggested early causal pathomechanisms and late compensatory adjustments.
382 A disease signature common to the three CNM forms was defined, suggesting a common
383 pathomechanism for CNM independent of the mutated genes. Comparison of the molecular effect of the
384 different therapies revealed a correlation between the molecular normalization and the phenotypic rescue.
385 In addition, novel potential therapeutic targets were suggested. Further molecular and biochemical

386 investigations identified several biomarkers for disease state and therapy efficacy in muscle (RNA,
387 proteins) and in plasma.
388
389 **Pathomechanism of centronuclear myopathies**
390 We compared the muscle transcriptomes of the *Mtm1*$^{-/y}$, *Bin1*$^{mck-/-}$ and *Dnm2*$^{SL/+}$ mice faithfully
391 reproducing the muscle weakness and histological hallmarks of the three main CNM forms [28, 49]. The
392 overall transcriptomes easily distinguished the CNM models from their WT littermates.
393 For MTM1-CNM, to identify the specific disease signature independent from the genetic backgrounds
394 or environment, we increased data heterogeneity by characterizing several *Mtm1*$^{-/y}$ groups on 129Pas,
395 C57BL/6J or mixed backgrounds bred in different animal houses, and then focused on the common
396 transcriptome dysregulation. Next, this signature was compared to available transcriptome data from one
397 MTM1 canine model and to a partial microarray analysis (4200 genes) of patient muscle biopsies [45, 46].
398 Our conclusions were supported by previous findings. Dysregulation of NMJ components (CHRNA1,
399 CHRND, CHRNG) were recently reported in the MTM1 dog and alteration of NMJ function was
400 suggested in a *mtm1* knockdown zebrafish and in *Mtm1* mouse models [46, 50, 51]. We found a high increase
401 in *Sln* expression in the three CNM mouse models, and upregulation of *Sln* was previously reported
402 following microarray analysis of the *Mtm1*$^{-/y}$ mouse [49]. In addition, longitudinal analyses of the muscle
403 transcriptome and proteome of *Mtm1*$^{-/y}$ mice at pre-symptomatic (E18.5), early (2 w) and late (7 w)
404 disease stages highlighted the same dysregulated pathways, although the same dysregulated
405 genes/proteins were not necessarily found (Figures 3, 4). These ages were chosen to potentially
406 distinguish between early causes of the disease and late consequences or compensatory mechanisms.
407 Further functional investigations are needed to confirm their causality. In addition, the proteome analysis
408 only covered the most abundant proteins. For example, BIN1 and DNM2 were not detected in the muscle
409 proteomes. However, BIN1 and DNM2 proteins were both increased in *Mtm1*$^{-/y}$ mice using specific
410 antibodies by western blot (Table 3)[34, 39]. Interestingly, we recently showed that the *Mtm1*$^{-/y}$ mice can be

411 rescued by either decreasing DNM2 or increasing BIN1 [37, 39], strongly supporting the idea that DNM2
412 increase is a disease cause while BIN1 increase is a compensatory mechanism.
413 The comparison of the *Mtm1*$^{-/y}$, *Bin1*$^{mck-/-}$ and *Dnm2*$^{SL/+}$ muscle transcriptomes revealed a common
414 disease signature, encompassing sarcomere organization, muscle contraction, muscle development and
415 cell adhesion. All these pathways were already the main ones found dysregulated at 2 w in *Mtm1*$^{-/y}$ mice,
416 supporting the hypothesis that their dysregulation represents the main pathomechanism for all CNM
417 forms (Figures 3, 4, 5). In addition to these pathways, inflammation activation (transcriptome) and
418 ribosomal biogenesis (proteome) were found only at 7 w suggesting that their dysregulation is a
419 consequence or a response to the disease state. Based on these data and on the knowledge that the three
420 CNM proteins regulate membrane remodeling, we propose a model for the pathomechanism of CNM.
421 Alteration of the triad membrane structure would lead to impaired calcium signaling and defective
422 muscle contraction, explaining the strong muscle weakness and hypotonia seen in patients. The myofiber
423 hypotrophy seen in patients and mouse models correlates with alteration of muscle development and
424 regeneration RNA markers, and may be related to dysregulation of IGF modulators as IGFBP2 or/and to
425 the reported decrease in satellite cells in patients [52]. The strong myofiber hypotrophy would then trigger
426 a later adaptation on protein homeostasis, as underlined by the increase of the ribosome biogenesis genes
427 found only at 7 w. Indeed, defects of protein homeostasis correlate with the alteration of autophagy and
428 the ubiquitin-proteasome pathways found in *Mtm1*$^{-/y}$ mice [25, 53, 54]. In parallel, a primary defect in cell
429 adhesion would impact the basement membrane and mechanotransduction and may explain defects in
430 muscle contraction and also the altered fiber shape found in patients and mice. This is in agreement with
431 the accumulation of integrins in *Mtm1*$^{-/y}$ mouse and patient myofibers, and with the proposed link
432 between MTM1 and beta integrin recycling [39, 55, 56]. The observed increased in interfiber space, together
433 with the alteration of muscle regeneration, would cause the late increase in genes implicated in
434 inflammation activation. As we detected a significant increase in RNA markers of inflammatory cells
435 while performing whole tissue RNAseq, we conclude there is a significant infiltration of inflammatory

cells that was confirmed by immunofluorescence labelling and quantification (Figure 5d-e). An inflammatory component was not previously reported for CNM but is common in dystrophies [57]. Furthermore, the dysregulated pathways found here were barely underlined previously in the other CNM forms linked to *BIN1* or *DNM*. Overall, although some of these pathways were previously found altered in MTM1-CNM, these omics analyses allowed to obtain a more complete and detailed overview of the pathomechanisms and extend it to several other CNMs. The GO term analysis of the common disease signature identified here for different CNM forms mostly reflects general muscle dysfunction and compensatory mechanisms put in place by the myofibers to cope with these defects, and thus highlights pathways also dysregulated in a large number of muscle diseases. However, differences appear when looking at the gene level that may reveal plasticity to impact or compensate the main muscle pathways depending on the sub-class of myopathies and on the primary genetic defect.

To a greater extent, we found several genes mutated in different neuromuscular diseases in the common CNM disease signature. Notably, *LMNA* is mutated in Emery-Dreifuss muscular dystrophy and the encoded protein lamin A/C regulates nuclear envelope stability (MIM#181350, 616516) [58]. Of note, lamin A/C and BIN1 both bind the LINC complex that regulates nuclear shape and positioning and BIN1-CNM patients have an altered nuclear envelope structure [59]. *KLHL40* is mutated in another congenital myopathy and is a substrate adaptor for the E3-ubiquitin ligase Cullin-3 (MIM#615348) [60, 61]. Similarly, MTM1 binds the Cullin-3 partner UBQLN2 and MTM1-CNM is linked to defects in the ubiquitin-proteasome pathway [54]. Several dysregulated genes in all CNM models are mutated in cardiomyopathy : *SCN5A* (MIM#601154), *TNNT2* (MIM#601494) and *MYL4* (MIM#617280). In addition, MYH2 and TNNC1 found upregulated in the proteome of 2 w *Mtm1*$^{-/y}$ mice are also mutated in a proximal myopathy (MIM#605637) or a cardiomyopathy (MIM#611879), respectively. Such findings are commonly observed in myopathies where upregulation of genes usually expressed in embryonic muscle or adult cardiac muscle are re-expressed in the affected skeletal muscle. Finally, *CHRNA1* (MIM#601462) and

460 *CHRND* (MIM#616322) are mutated in congenital myasthenic syndromes, correlating with the defect in
461 NMJ found in MTM1-CNM models [50, 51, 62].
462
463 **Common therapeutic targets for centronuclear myopathies**
464 We compared here three therapies involving three different targets in MTM1-CNM models, BIN1
465 overexpression, tamoxifen treatment and DNM2 regulation, and two methodologies for the latter target.
466 For the first time, this allows a molecular comparison of the different therapies for CNM. BIN1
467 overexpression appears to be the most efficient therapy to normalize the molecular defects. The
468 percentage of rescued genes varies greatly with 96% for BIN1 overexpression, 36% for DNM2
469 downregulation and 0.5% for tamoxifen in the MTM1-CNM mouse model. In the AAV-MTM1 treated
470 dogs, the percentage of rescued genes was 52% and 43% depending on the muscles analyzed [46]. These
471 findings highlight a correlation between the phenotypic and molecular rescue, as modulations of either
472 MTM1, BIN1 or DNM2 improved the lifespan, locomotor and histological phenotypes very efficiently,
473 while tamoxifen treatment resulted in a partial increase in lifespan and a significant amelioration of the
474 histopathology, although to a lesser extent than with genetic crosses [17, 31, 34, 37, 39-41]. As a potential
475 explanation to the different rescue efficiency of the transcriptome dysregulation, BIN1 may directly
476 modulate the general transcription program in a disease context, while MTM1 and DNM2 may directly
477 impact on the cellular (proteins, membrane) defects. Indeed, BIN1 binds the transcription factor MYC
478 and can shuttle between the cytoplasm and the nucleus in muscle cells [63-65]. Of note, BIN1 overexpression
479 was achieved through genetic cross and is thus chronic from embryogenesis, while AAV-MTM1 and
480 tamoxifen treatments are postnatal. However, transcriptomes comparison between chronic (*Dnm2*$^{+/-}$
481 genetic cross for MTM1-a) and acute DNM2 downregulation (ASO *Dnm2* injection for DNM2 and BIN1
482 cohorts) showed similar percentages of rescued genes: 36% in MTM1-a, 43% in DNM2 and 47% in
483 BIN1 cohorts (Figure 6). The rescuing effect of tamoxifen treatment is not based on transcriptome
484 remodeling but might directly involve membrane and protein functions.

We evaluated the toxicity of the different therapies used in this study by comparing the WT treated versus WT mice. Treatment of WT mice did not show a strong impact on the transcriptomes, while it was not reported in AAV-MTM1 treated dogs. For example, injection of ASO *Dnm2* decreased *Dnm2* expression but had few off-targets. No detectable phenotypic toxicity were observed in the treated WT mice. However, in human, even if the same gene will be targeted (either BIN1 or DNM2), the therapeutic compound and formulation may differ and the delivery method and corresponding dose will change. Here, for BIN1 overexpression we used the human cDNA while for DNM2 downregulation we used antisense oligonucleotides specific to the mouse *Dnm2* gene. We also detected the expected overexpression of the human *BIN1* gene in the MTM1-b cohort. BIN1 overexpression only changed the expression of three genes in the treated WT mice (Figure S9), while rescuing most transcriptome dysregulation in the *Mtm1*$^{-/y}$ mice, suggesting this therapy modulates the transcriptome mainly in a disease context (i.e. normalization).

The present data revealed several potential targets that were not directly targeted in the experiments (i.e. not MTM1, BIN1 nor DNM2). Genes of interest are expected to be dysregulated in disease and normalized upon efficient therapies, i.e. part of the therapy signature. In addition, known drugs targeting these gene products may be an asset, as it will allow drug repurposing and a faster clinical development. Several genes coding for subunits of the acetylcholine receptor are dysregulated. In particular acetylcholine esterase inhibitors used in clinical trial to treat myasthenic syndromes were tested with some success in different CNM forms [62]. *Scn5a* is also found upregulated in the disease signature and normalized in the therapy signature, and encodes a subunit of the sodium channel that can be inhibited by quinidine, a stereoisomer of quinine. *Mstn* encoding the myokine myostatin, an inhibitor of muscle growth, is significantly decreased in disease models of all cohorts except the *Bin1*$^{mck-/-}$ mouse (Log2FC = -0.6 while our threshold was -1). Inhibitors of myostatin are being tested in the clinic for other muscle diseases, and one of them (ActRIIB-mFc) showed only a very mild amelioration of the *Mtm1*$^{RC/y}$ knock-in mouse [66]. The mild amelioration can be explained by the fact that myostatin is already strongly

decreased in the disease state and thus could hardly be better suppressed [67]. *Sln* encoding the calcium regulator sarcolipin is strongly upregulated in disease models of all cohorts except the MTM1-c cohort. Reducing sarcolipin expression through genetic cross or shRNA improved Duchenne muscular dystrophy phenotypes in mice [68]. As a last example, myosins and troponins also meet these criteria and are targeted by several pharmacological regulators that may improve the muscle contraction defects of CNM. Indeed, all discussed modulations should be first validated in laboratory models, as it is unclear if dysregulation of some pathways are disease causing or compensatory.

Potential biomarkers for disease progression and therapy efficacy

We developed a strategy to identify potential biomarkers, combining RNAseq, RT-qPCR and western blotting in muscle with mass spectrometry and ELISA assays in blood, supported by database and literature mining. The validity of these biomarkers for monitoring disease progression and therapy efficacy has to be confirmed in human samples. This will require muscle and blood sampling of untreated and treated patients with different CNM forms together with adequate aged-matched controls. We found that *Mstn* RNA level is strongly decreased in *Mtm1*$^{-/y}$ and *Dnm2*$^{SL/+}$ mice and to a lesser extent in *Bin1*$^{mck-/-}$ (Log2FC=-0.6), and was normalized upon modulation of *MTM1*, *BIN1* and *Dnm2* (Figures S5, S9, S10, S11) [46]. In agreement, MSTN was recently found decreased in plasma from MTM1- and DNM2-CNM patients and responded to ASO *Dnm2* treatment in *Mtm1*$^{-/y}$ mice [69]. In addition, MSTN plasma level was also normalized upon BIN1 overexpression (Figure 7c). ANXA2 is a calcium-dependent phospholipid-binding protein that has a role in muscle repair [70], and was validated here as a muscle biomarker for all the CNM forms that we have tested. ANXA2 was detected in plasma, increased in the *Bin1*$^{mck-/-}$ mouse model, and normalized upon ASO *Dnm2* injection. Moreover, several reports cited ANXA2 to be a valuable biomarker in different cancers [71, 72].

In particular, these potential biomarkers could be used in clinical trials to monitor the progression/reversion of the disease or/and efficacy of the therapy. Currently, there are two clinical trials

ongoing to treat CNM. Firstly, the clinical trial (NCT03199469) for X-linked myotubular/centronuclear myopathy in patient under 5 years old based on *MTM1* gene replacement using AAV. Secondly, a clinical trial based on the decrease/normalization of *DNM2* with ASO (DYN101) is ongoing in patients with mutations in *MTM1* and *DNM2* over 16 years old (NCT04033159) and is planned for patients between 2 and 17 years old (NCT04743557).

Conclusions

Here, we report the first multi-omics analysis of animal models for several CNM forms, and of the effect of different therapies allowing to reveal a common disease signature and a common therapy signature. We determined the global pathological mechanism and deciphered the molecular impact of therapies. Longitudinal analyses of the treated and untreated MTM1-CNM model highlight potential causes and consequences of the pathology. In addition, we identified several novel biomarkers detectable in muscle and/or plasma through different validated methodologies. These findings and the associated data should be an asset to the community for further investigations. More generally, this study validates the concept of using omics to identify molecular signatures common to different disease forms or to several therapeutic strategies.

Materials and Methods

Animals

In this study we used different cohorts of mice. The sample size is given in Table S1. The cohort MTM1-a (WT, *Dnm2*$^{+/-}$, *Mtm1*$^{-/y}$, and *Mtm1*$^{-/y}$*Dnm2*$^{+/-}$) was previously phenotyped on a 129Pas genetic background [34]. The cohort MTM1-b (WT, Tg*BIN1*, *Mtm1*$^{-/y}$, and *Mtm1*$^{-/y}$Tg*BIN1*) was previously phenotyped on a 50% 129Pas and 50% C57BL/6N genetic background [39]. Both cohorts MTM1-a and MTM1-b were bred in IGBMC animal house in France. The cohort MTM1-c (WT, WT + tamoxifen, *Mtm1*$^{-/y}$, and *Mtm1*$^{-/y}$ + tamoxifen) was previously treated and phenotyped on a 129Pas genetic

560 background [40]. Tamoxifen was administered via supplement pellets of diet (30mg/kg of tamoxifen). This
561 cohort was bred in the animal house of the School of Pharmaceutical Sciences of the University of
562 Geneva, Switzerland. The cohort DNM2 (WT + ASO Ctrl, WT + ASO *Dnm2*, *Dnm2*$^{SL/+}$ + ASO Ctrl,
563 *Dnm2*$^{SL/+}$ + ASO *Dnm2*) was previously treated and phenotyped on a C57BL/6N genetic background [28].
564 The cohort BIN1 (WT + PBS, WT + ASO *Dnm2*, *Bin1*$^{mck/-}$ + PBS, *Bin1*$^{mck-/-}$ + ASO *Dnm2*) was
565 previously treated and phenotyped on a C57BL/6N genetic background (unpublished). Both DNM2 and
566 BIN1 cohorts were bred in IGBMC animal house in France. DNM2 and BIN1 cohorts were treated
567 weekly from 3 to 7 weeks of age with intraperitoneal injections of 25mg/kg of ASO (IONIS
568 Pharmaceuticals) targeting *Dnm2*. Only males were analyzed in this study as only *Mtm1*$^{-/y}$ males but not
569 *Mtm1*$^{+/-}$ females are affected. TA muscles were dissected at E18.5, 2w or 7w and obtained from the
570 previous studies. Data from MTM1-d cohort (WT, *Mtm1*$^{-/y}$) was retrieved from Maani *et al.* [41]. This
571 cohort was analyzed on a C57BL/6J genetic background and bred in University of Toronto animal house
572 in Canada. Quadriceps muscle from 5 w old animals were considered.
573
574 **Blood collection**
575 To collect plasma, blood samples were collected on EDTA-coated tubes (Microvette 500 K3E, Sarstedt)
576 by mandibular puncture. Samples were then centrifuged at +4°C during 10 min at 2,000 x *g*. To collect
577 serum, mandibular puncture was performed on mice. Blood was collected in a sterile empty tube and
578 kept for 30 min. After coagulation, only the supernatant (serum) was kept for further analysis. Plasma
579 and serum samples were stored at -80°C.
580
581 **RNA extraction and RNAseq**
582 RNA was extracted from Tibialis anterior muscles using TRI Reagent (Molecular Research Center,
583 Cincinnati, USA). RNA sequencing libraries were prepared using the TruSeq Stranded mRNA Sample

Preparation Kit and polyA selection and sequenced on a Hiseq4000 as single-end 50 bp reads for cohort MTM1-a, MTM1-b, MTMT1-c, cohort DNM2 and cohort BIN1.

Transcriptome analysis

Reads were preprocessed using cutadapt (version 1.10) in order to remove adapter, polyA and low-quality sequences (Phred quality score below 20). Reads shorter than 40 bases were excluded from further analysis. Reads were mapped to ERCC spike sequences (External RNA Controls Consortium) using bowtie version 2.2.8 and reads mapping to spike sequences were excluded from further analysis. Reads were mapped onto the mm10 assembly of *Mus musculus* genome using STAR version 2.5.3. Gene expression quantification was performed from uniquely aligned reads using htseq-count version 0.6.1p1, with annotations from Ensembl version 96 and union mode. Count tables were analyzed by the open-source RStudio environment for R and the Bioconductor software. DESeq2 package (version 1.16.1) was used to normalize, fit and compare the data between groups. Cutoff values for differential expressed genes determination were as follows: adjusted p-value < 0.05 and absolute value of Log 2 Fold Change > 1. This pipeline was used for cohort MTM1-a, MTM1-b, MTM1-c, DNM2, and BIN1.

To determine rescued genes, we developed a metric that quantifies the status of a diseased gene after the therapy. A diseased gene is defined as dysregulated in the comparison Disease *versus* WT (absolute value of Log 2 Fold Change > 1 & adjusted p-value < 0.05). The metric is calculated as the ratio between the Log 2 Fold Change of the two comparisons: Rescues *versus* Disease over Disease *versus* WT. We stratified the rescued genes into different categories: excessive rescue (metric > 120), not rescued (0 < metric < 30), partially rescued (30 < metric < 80) , rescued (80 < metric < 120) and worsened (metric < 0) (Figure S15).

Quantitative RT-PCR

Synthesis of cDNA was performed with SuperscriptTM IV Transcriptase (ThermoFischer Scientific, Whaltham, USA). Quantitative PCR was done in a Lightcycler® 480 (Roche Diagnostics, Basel,

609 Switzerland) with SYBR Green Master Mix I (Roche Diagnostics, Basel, Switzerland), and 0.5 µM of
610 forward and reverse primers. Primers were validated by amplicon sequencing and melting curve analysis
611 and listed in Table S17. *Stau1*, *Rps11* and *Rpl27* were used as housekeeping genes to normalize gene
612 expression.
613
614 **Protein extraction and Liquid digestion**
615 TA muscles were lysed in RIPA buffer supplemented with 1 mM PMSF, 1 mM DTT and complete mini-
616 EDTA-free protease inhibitor cocktail (Roche Diagnostics, Basel, Switzerland). DC Protein Assay Kit
617 (BioRad, Hercules, USA) was used to determine protein concentration. For serum analysis, most
618 abundant serum proteins were depleted with the Proteome purify 2 kit (MIDR002-020, R&D Systems)
619 according to manufacturer instructions before analysis by LC-MS/MS.
620 Protein mixtures were TCA-precipitated overnight at 4°C. Samples were then centrifuged at 14000 rpm
621 for 30 min at 4°C. Pellet were washed twice with 1 mL cold acetone and centrifuged at 14000 rpm for
622 10 min at 4°C. Washed pellets were then urea-denatured with 8 M urea in Tris-HCl 0.1 mM, reduced
623 with 5 mM TCEP for 30 min, and then alkylated with 10 mM iodoacetamide for 30 min in the dark. Both
624 reduction and alkylation were performed at room temperature and under agitation (850 rpm). Double
625 digestion was performed with endoproteinase Lys-C (Wako) at a ratio 1/100 (enzyme/proteins) in 8 M
626 urea for 4h, followed by an overnight modified trypsin digestion (Promega) at a ratio 1/100
627 (enzyme/proteins) in 2 M urea. Both Lys-C and Trypsin digestions were performed at 37°C. Peptide
628 mixtures were then desalted on C18 spin-column and dried on Speed-Vacuum before LC-MS/MS
629 analysis.
630
631 **LC-MS/MS Analysis**
632 Samples were analyzed using an Ultimate 3000 nano-RSLC (Thermo Scientific, San Jose California)
633 coupled in line with a LTQ-Orbitrap ELITE mass spectrometer via a nano-electrospray ionization source

(Thermo Scientific, San Jose California). Peptide mixtures were loaded on a C18 Acclaim PepMap100 trap-column (75 µm ID x 2 cm, 3 µm, 100Å, Thermo Fisher Scientific) for 3.5 min at 5 µL/min with 2% ACN, 0.1% FA in H2O and then separated on a C18 Accucore nano-column (75 µm ID x 50 cm, 2.6 µm, 150Å, Thermo Fisher Scientific) with a 90 min linear gradient from 5% to 35% buffer B (A: 0.1% FA in H2O / B: 99% ACN, 0.1% FA in H2O), then a 20 min linear gradient from 35% to 80% buffer B, followed with 5 min at 99% B and 5 min of regeneration at 5% B. The total duration was set to 120 min at a flow rate of 200 nL/min. The oven temperature was kept constant at 38°C.

The mass spectrometer was operated in positive ionization mode, in data-dependent mode with survey scans from m/z 350-1500 acquired in the Orbitrap at a resolution of 120,000 at m/z 400. The 20 most intense peaks (TOP20) from survey scans were selected for further fragmentation in the Linear Ion Trap with an isolation window of 2.0 Da and were fragmented by CID with normalized collision energy of 35%. Unassigned and single charged states were rejected.

The Ion Target Value for the survey scans (in the Orbitrap) and the MS2 mode (in the Linear Ion Trap) were set to 1E6 and 5E3 respectively and the maximum injection time was set to 100 msec for both scan modes. Dynamic exclusion was used. Exclusion duration was set to 20 sec, repeat count was set to 1 and exclusion mass width was ± 10 ppm.

Proteome analysis

Proteins were identified by database searching using Maxquant 1.6.6.0 and *Mus musculus* database (Uniprot Proteome database). Oxidation (M) was set as variable modification, and Carbamidomethylation (C) as fixed modification. Peptides were filtered with a false discovery rate (FDR) at 1%, the label-free quantitative values were processed using Perseus 1.6.6.0. 3521 proteins were identified. Statistical analyses were conducted in R-bioconductor (R-3.6.3). wrMisc, wrProteo packages were used to normalize, and to impute missing data with default parameters. Cutoff values for differential

expressed protein determination were as follows: adjusted p-value < 0.05 and absolute value Log 2 Fold Change > 1.

Western Blotting

Denaturation was performed on samples during 5 min at 95 °C with 5X Lane Reducing Buffer (ThermoFischer Scientific, Whaltham, USA) and loaded on 10% SDS-PAGE gel (161-0173, TGX Fast Cast Acrylamide kit, BioRad). Proteins were transferred to a nitrocellulose membrane using Transblot® TurboTM RTA Transfer Kit (BioRad, Hercules, USA). Loading was controlled by Ponceau S (P7170, Sigma-Aldrich) staining and Cy5 dye fluorophore (RPN4000, QuickStain). Membranes were blocked 1hr with 5% non-fat dry milk in 0.1% TBS Tween 20 prior to incubations with primary and secondary antibodies. The primary and secondary antibodies used were: ANXA2 (Mouse, 1:1000, sc-28385), CILP-1 (Rabbit, 1:1000, orb182643), FETUB (Rabbit, 1:500, orb252830), MTM1 (2827, 1:700, homemade [34]), BIN1 (R2405, 1:700, homemade [39]), DNM2 (DNM2-R2865, 1:500, homemade [34]), β-Actin (Mouse, 1:5000, homemade), peroxidase-coupled goat anti-rabbit (Goat, 1:10000, 112-036-062) and peroxidase-coupled goat anti-mouse (Goat, 1:10000, 115-036-068).

ELISA assays

Plasma proteins were quantified by Pierce BCA Protein Assay Kit (Thermo Fisher Scientific). Proteins (ANXA2, IGFBP2, CILP, MSTN) were quantified, using ANXA2 ELISA Kit (LS-F5798, LSBio), IGFBP2 ELISA Kit (ab207615, Abcam), CILP ELISA Kit (ABIN5591836, Antibodies-online), MSTN ELISA Kit (DGDF80, RD Systems) respectively, according to the manufacturer's instructions.

Muscle immunofluorescence

Transverse cryosections of TA muscles (8µm) were permeabilized with Triton 0.5%, blocked in BSA 5% and incubated overnight at +4°C with anti-CD68 (MCA1957GA BioRad, 1:100) for identifying

683 macrophages, DAPI for staining nuclei and wheat germ agglutinin (WGA) conjugated to alexa fluor AF-
684 647 for labeling the extracellular matrix. Slides were incubated with an anti-mouse secondary antibodies
685 for 1h at room temperature (A-11007 Thermo Fisher Scientific, 1:250), observed and photographed in
686 Leica DM 4000 Bx microscope. The images were analyzed using Image J software (n = 3 mice per
687 group).
688
689 **Orthologues retrieval and gene ontology analysis**
690 Orthologues between mice and dogs, human and mice were retrieved by bitr function in ClusterProfiler
691 package. Gene ontology analyses were performed with ClusterProfiler package (version 3.12.0) using
692 the overrepresentation test and the Benjamini–Hochberg correction for multiple testing. Enrichments
693 with a corrected p-value lower than 0.05 were considered significant [73].
694
695 **Data representation and statistical analyses**
696 PCA, volcano plot, qPCR results were generated in R-bioconductor (R-3.6.3). PCA was generated from
697 DESeq2 package (version 1.24.0) with variance stabilizing transformation. All genes were used to
698 generate the PCA from figures 3a and 4a. Disease signature genes (Table S9) were used to generate the
699 PCA from figure 5a. Therapy signature genes (Table S15) were used to generate the PCA from figure 6b.
700 Statistical analyses for RT-qPCR were performed by Dunn's multiple comparison test. Western blot and
701 ELISA results were analyzed in GraphPad Prism (v.9), using Student test. Venn diagrams were obtained
702 from InteractiVenn website (www.interactivenn.net)[74].
703
704 **Data availability**
705 The R script used to process the data has been deposited in GitLab and is freely available at
706 http://git.lbgi.fr/djeddi/Myomics. RNA-sequencing data were deposited in NCBI GEO with the
707 accession code GSE160084. The mass spectrometry proteomics data have been deposited to the

ProteomeXchange Consortium via the PRIDE partner repository with the dataset identifier PXD021725. The mass spectrometry proteomics data from the circulating proteins in serum, have been deposited to the ProteomeXchange Consortium via the PRIDE partner repository with the dataset identifier PXD021765.

Acknowledgements

We thank Luc Negroni, Bastien Morlet, Kirsley Chennen, Matthieu Jung for help in experiments and analyses, Genomeast for RNAseq, IGBMC platforms of proteomics and animal housing.

Authors' contributions

JL designed and supervised the study. SDjeddi performed most bioinformatics analyses with help from WR, CKeime and JT. SF, CKretz and OD provided mouse samples. DR, AM, SF and ASS performed RNA quantification. DR, SDjerroud and XMM performed western blots. DR performed ELISA assays. JDCN performed immunofluorescence. JL and SDjeddi wrote the manuscript.

Abbreviations

- AAV: Adeno-associated virus
- ASO: Antisense Oligonucleotides
- CNM: Centronuclear myopathies
- ELISA: Enzyme-linked Immunosorbent Assay
- GO: Gene Ontology
- IGF: Insulin Growth Factor
- Log2FC: Log2 Fold Change
- NMJ: Neuromuscular Junction
- PCA: Principal Component analysis

- PC: Principal Component

- RT-qPCR: Reverse Transcription Quantitative Polymerase Chain Reaction

- TA: Tibialis anterior

Competing interests

J.Laporte is co-founder of Dynacure (Illkirch, France).

Funding

This study was supported by institute funding from Institut National de la Santé et de la Recherche Médicale, Centre National de la Recherche Scientifique, Université de Strasbourg and by grants from the Agence Nationale de la Recherche ANR-10-LABX-0030-INRT, a French State fund managed by the Agence Nationale de la Recherche under the frame program Investissements d'Avenir ANR-10-IDEX-0002-02, Muscular Dystrophy Association (576154), Fondation pour la Recherche Médicale (201903007992), and Association Française contre les Myopathies-Téléthon (#20959 to OMD and JL and #22734 to JL).

References

1. Karczewski, KJ, and Snyder, MP (2018). Integrative omics for health and disease. Nat Rev Genet 19: 299-310.
2. Subramanian, I, Verma, S, Kumar, S, Jere, A, and Anamika, K (2020). Multi-omics Data Integration, Interpretation, and Its Application. Bioinform Biol Insights 14: 1177932219899051.
3. Jungbluth, H, Treves, S, Zorzato, F, Sarkozy, A, Ochala, J, Sewry, C, et al. (2018). Congenital myopathies: disorders of excitation-contraction coupling and muscle contraction. Nat Rev Neurol 14: 151-167.
4. Ravenscroft, G, Laing, NG, and Bonnemann, CG (2015). Pathophysiological concepts in the congenital myopathies: blurring the boundaries, sharpening the focus. Brain 138: 246-268.
5. Jungbluth, H, Wallgren-Pettersson, C, and Laporte, J (2008). Centronuclear (myotubular) myopathy. Orphanet J Rare Dis 3: 26.
6. Romero, NB (2010). Centronuclear myopathies: a widening concept. Neuromuscul Disord 20: 223-228.

7. Laporte, J, Hu, LJ, Kretz, C, Mandel, JL, Kioschis, P, Coy, JF, et al. (1996). A gene mutated in X-linked myotubular myopathy defines a new putative tyrosine phosphatase family conserved in yeast. Nat Genet 13: 175-182.
8. Bitoun, M, Maugenre, S, Jeannet, PY, Lacene, E, Ferrer, X, Laforet, P, et al. (2005). Mutations in dynamin 2 cause dominant centronuclear myopathy. Nat Genet 37: 1207-1209.
9. Bitoun, M, Bevilacqua, JA, Prudhon, B, Maugenre, S, Taratuto, AL, Monges, S, et al. (2007). Dynamin 2 mutations cause sporadic centronuclear myopathy with neonatal onset. Ann Neurol 62: 666-670.
10. Bohm, J, Biancalana, V, Dechene, ET, Bitoun, M, Pierson, CR, Schaefer, E, et al. (2012). Mutation spectrum in the large GTPase dynamin 2, and genotype-phenotype correlation in autosomal dominant centronuclear myopathy. Hum Mutat 33: 949-959.
11. Bohm, J, Biancalana, V, Malfatti, E, Dondaine, N, Koch, C, Vasli, N, et al. (2014). Adult-onset autosomal dominant centronuclear myopathy due to BIN1 mutations. Brain 137: 3160-3170.
12. Nicot, AS, Toussaint, A, Tosch, V, Kretz, C, Wallgren-Pettersson, C, Iwarsson, E, et al. (2007). Mutations in amphiphysin 2 (BIN1) disrupt interaction with dynamin 2 and cause autosomal recessive centronuclear myopathy. Nat Genet 39: 1134-1139.
13. Gonorazky, HD, Bonnemann, CG, and Dowling, JJ (2018). The genetics of congenital myopathies. Handb Clin Neurol 148: 549-564.
14. Schartner, V, Laporte, J, and Bohm, J (2019). Abnormal Excitation-Contraction Coupling and Calcium Homeostasis in Myopathies and Cardiomyopathies. J Neuromuscul Dis 6: 289-305.
15. Jungbluth, H, and Gautel, M (2014). Pathogenic mechanisms in centronuclear myopathies. Front Aging Neurosci 6: 339.
16. Hnia, K, Vaccari, I, Bolino, A, and Laporte, J (2012). Myotubularin phosphoinositide phosphatases: cellular functions and disease pathophysiology. Trends Mol Med 18: 317-327.
17. Tasfaout, H, Cowling, BS, and Laporte, J (2018). Centronuclear myopathies under attack: A plethora of therapeutic targets. J Neuromuscul Dis 5: 387-406.
18. Lawlor, MW, Beggs, AH, Buj-Bello, A, Childers, MK, Dowling, JJ, James, ES, et al. (2016). Skeletal Muscle Pathology in X-Linked Myotubular Myopathy: Review With Cross-Species Comparisons. J Neuropathol Exp Neurol 75: 102-110.
19. Beggs, AH, Bohm, J, Snead, E, Kozlowski, M, Maurer, M, Minor, K, et al. (2010). MTM1 mutation associated with X-linked myotubular myopathy in Labrador Retrievers. Proc Natl Acad Sci U S A 107: 14697-14702.
20. Bohm, J, Vasli, N, Maurer, M, Cowling, B, Shelton, GD, Kress, W, et al. (2013). Altered Splicing of the BIN1 Muscle-Specific Exon in Humans and Dogs with Highly Progressive Centronuclear Myopathy. PLoS Genet 9: e1003430.
21. Olby, NJ, Friedenberg, S, Meurs, K, DeProspero, D, Guevar, J, Lau, J, et al. (2020). A mutation in MTM1 causes X-Linked myotubular myopathy in Boykin spaniels. Neuromuscul Disord 30: 353-359.
22. Shelton, GD, Rider, BE, Child, G, Tzannes, S, Guo, LT, Moghadaszadeh, B, et al. (2015). X-linked myotubular myopathy in Rottweiler dogs is caused by a missense mutation in Exon 11 of the MTM1 gene. Skelet Muscle 5: 1.
23. Buj-Bello, A, Laugel, V, Messaddeq, N, Zahreddine, H, Laporte, J, Pellissier, JF, et al. (2002). The lipid phosphatase myotubularin is essential for skeletal muscle maintenance but not for myogenesis in mice. Proc Natl Acad Sci U S A 99: 15060-15065.
24. Pierson, CR, Dulin-Smith, AN, Durban, AN, Marshall, ML, Marshall, JT, Snyder, AD, et al. (2012). Modeling the human MTM1 p.R69C mutation in murine Mtm1 results in exon 4 skipping and a less severe myotubular myopathy phenotype. Hum Mol Genet 21: 811-825.
25. Fetalvero, KM, Yu, Y, Goetschkes, M, Liang, G, Valdez, RA, Gould, T, et al. (2013). Defective autophagy and mTORC1 signaling in myotubularin null mice. Mol Cell Biol 33: 98-110.

26. Chen, X, Gao, YQ, Zheng, YY, Wang, W, Wang, P, Liang, J, et al. (2020). The intragenic microRNA miR199A1 in the dynamin 2 gene contributes to the pathology of X-linked centronuclear myopathy. J Biol Chem 295: 8656-8667.
27. Durieux, AC, Vignaud, A, Prudhon, B, Viou, MT, Beuvin, M, Vassilopoulos, S, et al. (2010). A centronuclear myopathy-dynamin 2 mutation impairs skeletal muscle structure and function in mice. Hum Mol Genet 19: 4820-4836.
28. Munoz, XM, Kretz, C, Silva-Rojas, R, Ochala, J, Menuet, A, Romero, NB, et al. (2020). Physiological impact and disease reversion for the severe form of centronuclear myopathy linked to dynamin. JCI Insight 5.
29. Prokic, I, Cowling, BS, Kutchukian, C, Kretz, C, Tasfaout, H, Gache, V, et al. (2020). Differential physiological role of BIN1 isoforms in skeletal muscle development, function and regeneration. Dis Model Mech.
30. Muller, AJ, Baker, JF, DuHadaway, JB, Ge, K, Farmer, G, Donover, PS, et al. (2003). Targeted disruption of the murine Bin1/Amphiphysin II gene does not disable endocytosis but results in embryonic cardiomyopathy with aberrant myofibril formation. Mol Cell Biol 23: 4295-4306.
31. Childers, MK, Joubert, R, Poulard, K, Moal, C, Grange, RW, Doering, JA, et al. (2014). Gene therapy prolongs survival and restores function in murine and canine models of myotubular myopathy. Sci Transl Med 6: 220ra210.
32. Buj-Bello, A, Fougerousse, F, Schwab, Y, Messaddeq, N, Spehner, D, Pierson, CR, et al. (2008). AAV-mediated intramuscular delivery of myotubularin corrects the myotubular myopathy phenotype in targeted murine muscle and suggests a function in plasma membrane homeostasis. Hum Mol Genet 17: 2132-2143.
33. Raess, MA, Cowling, BS, Bertazzi, DL, Kretz, C, Rinaldi, B, Xuereb, JM, et al. (2017). Expression of the neuropathy-associated MTMR2 gene rescues MTM1-associated myopathy. Hum Mol Genet 26: 3736-3748.
34. Cowling, BS, Chevremont, T, Prokic, I, Kretz, C, Ferry, A, Coirault, C, et al. (2014). Reducing dynamin 2 expression rescues X-linked centronuclear myopathy. J Clin Invest 124: 1350-1363.
35. Cowling, BS, Prokic, I, Tasfaout, H, Rabai, A, Humbert, F, Rinaldi, B, et al. (2017). Amphiphysin (BIN1) negatively regulates dynamin 2 for normal muscle maturation. J Clin Invest 127: 4477-4487.
36. Buono, S, Ross, JA, Tasfaout, H, Levy, Y, Kretz, C, Tayefeh, L, et al. (2018). Reducing dynamin 2 (DNM2) rescues DNM2-related dominant centronuclear myopathy. Proc Natl Acad Sci U S A.
37. Tasfaout, H, Buono, S, Guo, S, Kretz, C, Messaddeq, N, Booten, S, et al. (2017). Antisense oligonucleotide-mediated Dnm2 knockdown prevents and reverts myotubular myopathy in mice. Nat Commun 8: 15661.
38. Tasfaout, H, Lionello, VM, Kretz, C, Koebel, P, Messaddeq, N, Bitz, D, et al. (2018). Single Intramuscular Injection of AAV-shRNA Reduces DNM2 and Prevents Myotubular Myopathy in Mice. Mol Ther 26: 1082-1092.
39. Lionello, VM, Nicot, AS, Sartori, M, Kretz, C, Kessler, P, Buono, S, et al. (2019). Amphiphysin 2 modulation rescues myotubular myopathy and prevents focal adhesion defects in mice. Sci Transl Med 11.
40. Gayi, E, Neff, LA, Massana Munoz, X, Ismail, HM, Sierra, M, Mercier, T, et al. (2018). Tamoxifen prolongs survival and alleviates symptoms in mice with fatal X-linked myotubular myopathy. Nat Commun 9: 4848.
41. Maani, N, Sabha, N, Rezai, K, Ramani, A, Groom, L, Eltayeb, N, et al. (2018). Tamoxifen therapy in a murine model of myotubular myopathy. Nat Commun 9: 4849.
42. Biressi, S, Molinaro, M, and Cossu, G (2007). Cellular heterogeneity during vertebrate skeletal muscle development. Dev Biol 308: 281-293.

43. Egerman, MA, and Glass, DJ (2014). Signaling pathways controlling skeletal muscle mass. Crit Rev Biochem Mol Biol 49: 59-68.
44. Bismuth, K, and Relaix, F (2010). Genetic regulation of skeletal muscle development. Exp Cell Res 316: 3081-3086.
45. Noguchi, S, Fujita, M, Murayama, K, Kurokawa, R, and Nishino, I (2005). Gene expression analyses in X-linked myotubular myopathy. Neurology 65: 732-737.
46. Dupont, JB, Guo, J, Renaud-Gabardos, E, Poulard, K, Latournerie, V, Lawlor, MW, et al. (2020). AAV-Mediated Gene Transfer Restores a Normal Muscle Transcriptome in a Canine Model of X-Linked Myotubular Myopathy. Mol Ther 28: 382-393.
47. Vissing, J, Johnson, K, Topf, A, Nafissi, S, Diaz-Manera, J, French, VM, et al. (2019). POPDC3 Gene Variants Associate with a New Form of Limb Girdle Muscular Dystrophy. Ann Neurol 86: 832-843.
48. Jiang, L, Wang, M, Lin, S, Jian, R, Li, X, Chan, J, et al. (2020). A Quantitative Proteome Map of the Human Body. Cell 183: 269-283 e219.
49. Al-Qusairi, L, Weiss, N, Toussaint, A, Berbey, C, Messaddeq, N, Kretz, C, et al. (2009). T-tubule disorganization and defective excitation-contraction coupling in muscle fibers lacking myotubularin lipid phosphatase. Proc Natl Acad Sci U S A 106: 18763-18768.
50. Mercier, L, Bohm, J, Fekonja, N, Allio, G, Lutz, Y, Koch, M, et al. (2016). In vivo imaging of skeletal muscle in mice highlights muscle defects in a model of myotubular myopathy. Intravital 5: e1168553.
51. Dowling, JJ, Joubert, R, Low, SE, Durban, AN, Messaddeq, N, Li, X, et al. (2012). Myotubular myopathy and the neuromuscular junction: a novel therapeutic approach from mouse models. Dis Model Mech 5: 852-859.
52. Shichiji, M, Biancalana, V, Fardeau, M, Hogrel, JY, Osawa, M, Laporte, J, et al. (2013). Extensive morphological and immunohistochemical characterization in myotubular myopathy. Brain Behav 3: 476-486.
53. Al-Qusairi, L, Prokic, I, Amoasii, L, Kretz, C, Messaddeq, N, Mandel, JL, et al. (2013). Lack of myotubularin (MTM1) leads to muscle hypotrophy through unbalanced regulation of the autophagy and ubiquitin-proteasome pathways. FASEB J 27: 3384-3394.
54. Gavriilidis, C, Laredj, L, Solinhac, R, Messaddeq, N, Viaud, J, Laporte, J, et al. (2018). The MTM1-UBQLN2-HSP complex mediates degradation of misfolded intermediate filaments in skeletal muscle. Nat Cell Biol 20: 198-210.
55. Velichkova, M, Juan, J, Kadandale, P, Jean, S, Ribeiro, I, Raman, V, et al. (2010). Drosophila Mtm and class II PI3K coregulate a PI(3)P pool with cortical and endolysosomal functions. J Cell Biol 190: 407-425.
56. Ketel, K, Krauss, M, Nicot, AS, Puchkov, D, Wieffer, M, Muller, R, et al. (2016). A phosphoinositide conversion mechanism for exit from endosomes. Nature 529: 408-412.
57. Chazaud, B (2020). Inflammation and Skeletal Muscle Regeneration: Leave It to the Macrophages! Trends Immunol 41: 481-492.
58. Chatzifrangkeskou, M, Bonne, G, and Muchir, A (2015). Nuclear envelope and striated muscle diseases. Curr Opin Cell Biol 32: 1-6.
59. D'Alessandro, M, Hnia, K, Gache, V, Koch, C, Gavriilidis, C, Rodriguez, D, et al. (2015). Amphiphysin 2 Orchestrates Nucleus Positioning and Shape by Linking the Nuclear Envelope to the Actin and Microtubule Cytoskeleton. Dev Cell 35: 186-198.
60. Garg, A, O'Rourke, J, Long, C, Doering, J, Ravenscroft, G, Bezprozvannaya, S, et al. (2014). KLHL40 deficiency destabilizes thin filament proteins and promotes nemaline myopathy. J Clin Invest 124: 3529-3539.

61. Ravenscroft, G, Miyatake, S, Lehtokari, VL, Todd, EJ, Vornanen, P, Yau, KS, et al. (2013). Mutations in KLHL40 are a frequent cause of severe autosomal-recessive nemaline myopathy. Am J Hum Genet 93: 6-18.
62. Robb, SA, Sewry, CA, Dowling, JJ, Feng, L, Cullup, T, Lillis, S, et al. (2011). Impaired neuromuscular transmission and response to acetylcholinesterase inhibitors in centronuclear myopathies. Neuromuscul Disord 21: 379-386.
63. Cassimere, EK, Pyndiah, S, and Sakamuro, D (2009). The c-MYC-interacting proapoptotic tumor suppressor BIN1 is a transcriptional target for E2F1 in response to DNA damage. Cell Death Differ 16: 1641-1653.
64. Sakamuro, D, Elliott, KJ, Wechsler-Reya, R, and Prendergast, GC (1996). BIN1 is a novel MYC-interacting protein with features of a tumour suppressor. Nat Genet 14: 69-77.
65. Wechsler-Reya, RJ, Elliott, KJ, and Prendergast, GC (1998). A role for the putative tumor suppressor Bin1 in muscle cell differentiation. Mol Cell Biol 18: 566-575.
66. Lawlor, MW, Read, BP, Edelstein, R, Yang, N, Pierson, CR, Stein, MJ, et al. (2011). Inhibition of activin receptor type IIB increases strength and lifespan in myotubularin-deficient mice. Am J Pathol 178: 784-793.
67. Mariot, V, Joubert, R, Hourde, C, Feasson, L, Hanna, M, Muntoni, F, et al. (2017). Downregulation of myostatin pathway in neuromuscular diseases may explain challenges of anti-myostatin therapeutic approaches. Nat Commun 8: 1859.
68. Voit, A, Patel, V, Pachon, R, Shah, V, Bakhutma, M, Kohlbrenner, E, et al. (2017). Reducing sarcolipin expression mitigates Duchenne muscular dystrophy and associated cardiomyopathy in mice. Nat Commun 8: 1068.
69. Koch, C, Buono, S, Menuet, A, Robe, A, Djeddi, S, Kretz, C, et al. (2020). Myostatin: a Circulating Biomarker Correlating with Disease in Myotubular Myopathy Mice and Patients. Mol Ther Methods Clin Dev 17: 1178-1189.
70. Bittel, DC, Chandra, G, Tirunagri, LMS, Deora, AB, Medikayala, S, Scheffer, L, et al. (2020). Annexin A2 Mediates Dysferlin Accumulation and Muscle Cell Membrane Repair. Cells 9.
71. Tas, F, Tilgen Yasasever, C, Karabulut, S, Tastekin, D, and Duranyildiz, D (2015). Circulating annexin A2 as a biomarker in gastric cancer patients: correlation with clinical variables. Biomed Pharmacother 69: 237-241.
72. Sharma, MC (2019). Annexin A2 (ANX A2): An emerging biomarker and potential therapeutic target for aggressive cancers. Int J Cancer 144: 2074-2081.
73. Yu, G, Wang, LG, Han, Y, and He, QY (2012). clusterProfiler: an R package for comparing biological themes among gene clusters. OMICS 16: 284-287.
74. Heberle, H, Meirelles, GV, da Silva, FR, Telles, GP, and Minghim, R (2015). InteractiVenn: a web-based tool for the analysis of sets through Venn diagrams. BMC Bioinformatics 16: 169.

Figure Legends

Figure 1. Experimental design. **(a)** Timeline of the different steps occurring during muscle development in mice. The green arrow represents the normal lifespan of control mice (WT). The phenotype of the three mouse models (*Mtm1*$^{-/y}$, *Bin1*$^{mck/-}$, *Dnm2*$^{SL/+}$) used in this study is illustrated by the colored arrows with a color gradient ranging from green for non-affected mice, yellow for the onset of myopathy and red for affected mice. **(b)** Molecular analyses were performed on different mouse models, *Mtm1*$^{-/y}$,

951 *Bin1*$^{mck/-}$, *Dnm2*$^{SL/+}$, untreated or treated by different therapeutic approaches (overexpression of *BIN1*,
952 tamoxifen supplementation or downregulation of *Dnm2* either by genetic cross or by ASO injection).
953 Disease signature refers to the common dysregulated genes in the three mouse models compared to WT
954 littermates, while the therapy signature refers to the common genes rescued following the different
955 treatments.
956
957 **Figure 2.** MTM1-CNM signature in different species. **(a)** Venn diagram illustrating the shared
958 dysregulated genes based on the *Mtm1*$^{-/y}$ vs WT comparison of four mouse cohorts. The percentages of
959 uniquely dysregulated genes and the number of differentially expressed genes in each cohort are
960 indicated in brackets. **(b)** Gene Ontology (GO) enrichment analysis of differentially expressed genes
961 common to the four *Mtm1*$^{-/y}$ mouse cohorts. The 20 GO biological process terms with the lowest p-value
962 are displayed. **(c)** Venn diagram illustrating the shared dysregulated genes based on MTM1 vs control
963 comparison in three different species: human, mice (TA) and dog (*Vastus lateralis*). **(d)** mRNA
964 log2foldchange expression of differentially expressed genes common to the three species. **(e)** GO
965 enrichment analysis of differentially expressed genes common to mice and dog. The 20 GO biological
966 process terms with the lowest p-value are displayed. **(f)** mRNA log2foldchange expression of
967 differentially expressed genes common between mice and dog determined by RNAseq (dog, mice) and
968 RT-qPCR (mice).
969
970 **Figure 3.** Longitudinal mRNA profiling of *Mtm1*$^{-/y}$ mice. **(a)** Principal component analysis of RNAseq
971 data. The first and fourth axes are represented. Colored symbols represent genotypes and shapes represent
972 ages for each mouse. **(b)** Venn diagram illustrating the shared and specific dysregulated genes based on
973 the *Mtm1*$^{-/y}$ vs WT comparison at 2 and 7 weeks. The most enriched GO biological processes are
974 represented by dashed boxes. **(c)** Volcano plots representing the differentially expressed genes at 2w and
975 **(d)** at 7w. Up-regulated genes are in red and down-regulated genes are in blue. **(e)** Gene expression data

(log normalized counts) determined by RNASeq for *Mstn* (muscle growth), *Sln* (calcium homeostasis), *Ahnak2 (*sarcomere organization), *Myl4* and *Tnnt2* (muscle contraction)*, Itga3* (cell adhesion), *Cxc3cl1* and*Tlr2* (inflammation pathway) across time. Each dot represents an individual mouse, the shaded area represents the confidence interval at 0.95.

Figure 4. Longitudinal protein profiling of *Mtm1*$^{-/y}$ mice. (**a)** Principal component analysis of mass spectrometry data. Colored symbols represent genotypes and shapes represent ages for each mouse. Technical and biological replicates are shown. **(b)** Venn diagram illustrating the shared and specific dysregulated proteins based on the *Mtm1*$^{-/y}$ vs WT comparison at 2 and 7 weeks; the most enriched GO biological processes are represented by dashed boxes. **(c)** Volcano plots displaying the differentially expressed proteins at 2w and **(d)** at 7w. Up-regulated proteins are in red and down-regulated proteins are in blue. **(e)** MYH2 and TNNC1 (muscle contraction), and RPL3 (ribosomal biogenesis) expression data obtained by mass spectrometry across time. Each dot represents technical and biological replicates, the shaded areas represent the confidence interval at 0.95.

Figure 5. CNM disease signature in mouse. **(a)** PCA on RNAseq data on the 155 genes commonly differentially expressed between the five cohorts, each dot represents a mouse. The three different CNM mouse models are represented by red, orange, yellow dots and the WT controls by green dots. **(b)** Venn diagram illustrating the shared and specific dysregulated genes between the five CNM cohorts. **(c)** GO enrichment analysis for biological processes (BP), cellular component (CC) and molecular function (MF) of the 155 common differentially expressed genes between the five CNM cohorts. GO terms with highest ratio and lowest q-value are represented. The ratio represents the number of genes dysregulated divided by the total number of genes in the category. The color scale is based on the q-value, dark colors indicate most significantly over-represented terms, while lighter colors indicate the least significant terms. **(d)** Macrophage localization by immunofluorescence in transversal section from TA muscle at 7 w in

Mtm1$^{-/y}$, *Bin1*$^{mck-/-}$ and *Dnm2*$^{SL/+}$ mice. Nuclei: DAPI (blue), macrophages (red), plasma membrane (WGA, yellow). Arrowheads point to macrophages. Scale bar = 100 µm. **(e)** Quantification of macrophages. T-test; *p < 0.05, **p < 0.01. **(f)** Transcriptomic expression changes between diseased and WT mice for the 5 cohorts. The log2foldchange expression of *Anxa2*, *Cilp*, *Fetub*, *Fgfr4*, *Fst*, *Igfbp2*, *Mstn*, *Myl4*, *Runx1*, *S100a4*, *Serpinb1a*, *Sln*, *Sox11*, *Tnnt2* are represented by the bars.

Figure 6. Common therapy signature in CNM mice treated with different therapies. **(a)** PCA on RNAseq data of the 42 genes commonly rescued in the four cohorts. Each symbol represents a mouse. The three different CNM mouse models are represented by red, orange and yellow colors and the WT controls are represented in green**.** Treatments are represented by different symbols: squares for the downregulation of *Dnm2,* either by ASO injection (full square) or by genetic cross (boxed +), the triangle represents the overexpression of human *BIN1*, the cross represents the administration of tamoxifen. **(b)** Venn diagram illustrating the shared and specific dysregulated genes between rescued and diseased mice in each mouse cohort. **(c)** mRNA expression levels of *Anxa2*, *Cilp*, *Fetub*, *Igfbp2* in CNM mice either diseased or rescued upon therapy, and in untreated and treated controls. Boxplots displaying normalized Ct values. Pairwise significance with p-value < 0.05 calculated by Dunn's Test are represented in bold. **(d)** Among the 42 genes identified in the therapy signature, 35 have human orthologs and 2 (*Scn5a* and *Sbk3*) encode proteins targeted by known drugs.

Figure 7. Muscle and circulating biomarkers for disease and rescue states. **(a)** Venn diagram illustrating the strategy to extract biomarkers from the comparison of disease and therapy signatures, proteins detected by mass spectrometry in the sera of WT mice, public databases (GTEx, BioGPS, Illumina, GXD), and literature. **(b)** Protein levels of ANXA2, FETUB and CILP in Gastrocnemius with standardization by rouge Ponceau red staining in *Mtm1*$^{-/y}$ (Cohort MTM1-a), *Bin1*$^{mck-/-}$ and *Dnm2*$^{SL/+}$ mouse models at 7 w. Protein levels are represented as the fold difference from the average of the WT

(4 ≤ n ≤ 9). Student test; *p < 0.05, **p < 0.01, ***p < 0.001. **(c)** Plasma levels of IGFBP2, ANXA2, CILP and MSTN (ng/mg or pg/mg protein total) from untreated and treated *Mtm1*$^{-/y}$, *Bin1*$^{mck-/-}$ and *Dnm2*$^{SL/+}$ mouse models and WT controls (3 ≤ n ≤ 12). Student test for untreated cohorts; **p < 0.01. Tukey's test for treated cohorts; *p < 0.05, **p < 0.01, ***p < 0.001.

Table 1: Description of the mouse cohorts used in the study. Country, age, background, muscle and sequencer used.

Table 2: List of the most dysregulated genes in MTM1-CNM mice.

Table 3: RNA and protein levels of *Mtm1* (MTM1), *Bin1* (BIN1) and *Dnm2* (DNM2) in *Mtm1*$^{-/y}$, *Bin1*$^{mck-/-}$, *Dnm2*$^{SL/+}$ and *Dnm2*$^{RW/+}$ mice.

Supplementary information:

Table S1. Number of mice included in the different cohorts for transcriptomic and proteomic experiments.

Table S2. List of the 287 genes commonly differentially expressed in MTM1-CNM cohorts (Fig 2a).

Table S3. List of the 632 genes differentially expressed in common for MTM1-a, MTM1-b and MTM1-c cohorts.

Table S4. List of the specific dysregulated genes expressed in MTM1-CNM cohorts (Fig 2c).

Table S5. List of the 68 differentially expressed genes common between mice (Tibialis anterior) and dogs (Vastus Lateralis).

Table S6. List of the 53 differentially expressed genes common between mice (Tibialis anterior) and dogs (Biceps Femoris).

Table S7. List of DEGs in cohort MTM1-a.

Table S8. List of DEP Mtm1−/y vs WT (Cohort MTM1-a)

Table S9. List of the 155 common differentially expressed genes for the MTM1-a, MTM1-b, MTM1-c, DNM2 and BIN1 cohorts.

Table S10. List of DEGs in cohort MTM1-b.

Table S11. List of DEGs in cohort MTM1-c.

Table S12. List of DEGs in cohort DNM2.

Table S13. List of DEGs in cohort BIN1.

Table S14. List of the specific dysregulated genes expressed in MTM1, DNM2 and BIN1 cohorts (Fig 5b).

Table S15. List of the 42 common differentially expressed genes for the MTM1-a, MTM1-b, DNM2 and BIN1 cohorts.

Table S16. List of proteins retrieved by mass spectrometry in serum of WT mice at 8 w.

Table S17. List of primers used for RT-qPCR.

Figure S1. (a) Venn diagram illustrating the common dysregulated genes based on the MTM1 vs controls comparison in three different species: human, mice and dog (Biceps femoris). **(b-c)** Gene Ontology (GO) enrichment analysis of the specific differentially expressed genes in **(b)** Human cohort and **(c)** in Dog cohort. The 20 GO biological process terms with the lowest p-value are displayed.

Figure S2. PCA related to Fig 5b. **(a)** PC1 and PC2 and **(b)** PC1 and PC3 are represented.

Figure S3. GO enrichment analysis for biological processes (BP), cellular component (CC) and molecular function (MF) of the differentially expressed genes in *Mtm1*$^{-/y}$ vs WT mice (N =1175 genes) at **(a)** 2 w and **(b)** at 7 w (N=1981 genes). GO terms with highest ratio and lowest q-value are represented. The ratio represents the number of genes dysregulated divided by the total number of genes in the

category. The color scale is based on the q-value, dark colors indicate most significantly over-represented terms, while lighter colors indicate the least significant terms.

Figure S4. mRNA expression levels of genes of interest in diseased, rescued and control mice in the MTM1-a cohort at 2 w. Boxplots displaying normalized Ct values. Pairwise significance calculated by Dunn's test, $p < 0.05$ are represented in bold.

Figure S5. mRNA expression levels of genes of interest in diseased, rescued and control mice in the MTM1-a cohort at 7 w. Boxplots displaying normalized Ct values. Pairwise significance calculated by Dunn's test, $p < 0.05$ are represented in bold.

Figure S6. GO enrichment analysis for biological processes (BP), cellular component (CC) and molecular function (MF) of the differentially expressed proteins in *Mtm1*$^{-/y}$ vs WT mice (N =168 proteins) at **(a)** 2w and **(b)** at 7 w (N=496 proteins). GO terms with highest ratio and lowest q-value are represented. The ratio represents the number of proteins dysregulated divided by the total number of proteins in the category. The color scale is based on the q-value, dark colors indicate most significantly over-represented terms, while lighter colors indicate the least significant terms.

Figure S7. Pearson correlation between mRNA and protein levels measured by RNASeq and mass spectrometry **(a)** at 2 w and **(b)** at 7 w**.**

Figure S8. MTM1 and BIN1 protein levels in *Dnm2*$^{SL/+}$ Tibialis anterior muscles. MTM1, BIN1 and DNM2 protein levels in *Dnm2*$^{RW/+}$ TA muscles. MTM1 protein level in *Bin1*$^{mck-/-}$ TA muscles. Pairwise significance calculated by t-test, $p < 0.05$ are represented in bold.

Figure S9. Number of dysregulated genes and the associated PCA for each cohort for four comparisons (Disease vs WT, Disease vs Rescue, Rescue vs Disease, and WT treated vs WT). **(a)** Cohort MTM1-b. **(b)** Cohort MTM1-c. **(c)** Cohort DNM2. **(d)** Cohort BIN1.

Figure S10. mRNA expression levels of genes of interest in diseased, rescued and control mice in the DNM2 cohort at 7 w. Boxplots displaying normalized Ct values. Pairwise significance calculated by Dunn's test, $p < 0.05$ are represented in bold.

Figure S11. mRNA expression levels of genes of interest in diseased, rescued and control mice in the MTM1-b cohort at 7 w. Boxplots displaying normalized Ct values. Pairwise significance calculated by Dunn's test, $p < 0.05$ are represented in bold.

Figure S12. mRNA expression levels of genes of interest in diseased, rescued and control mice in the BIN1 cohort at 7 w. Boxplots displaying normalized Ct values. Pairwise significance calculated by Dunn's test, $p < 0.05$ are represented in bold.

Figure S13. Gene Ontology (GO) enrichment analysis of the specific differentially expressed genes **(a)** in MTM1 cohort **(b)** in BIN1 cohort and **(c)** in DNM2 cohort. The 20 GO biological process terms with the lowest p-value are displayed.

Figure S14. Blot related to Fig 7b.

Figure S15. (a) Histogram displaying the proportion of genes according to their status and the metric per cohort. **(b)** Barplot showing the number of genes dysregulated and the status of these genes through the different therapies.

Table1: Description of the mouse cohorts used in the study. Country, age, background, muscle and sequencer used.

	Country	Age	Background	Muscle	Sequencer
Cohort MTM1-a	France	7w	129Pas	Tibialis anterior	Hiseq4000
Cohort 2 MTM1-b	France	7w	50% 129Pas; 50% C57BL/6N	Tibialis anterior	Hiseq4000
Cohort 3 MTM1-c	Switzerland	7w	129Pas	Tibialis anterior	Hiseq4000
Cohort 4 MTM1-d	Canada (Maani et al., 2018)	5w	C57BL/6J	Quadriceps	Hiseq2500
Cohort DNM2	France	7w	C57BL/6N	Tibialis anterior	Hiseq4000
Cohort BIN1	France	7w	C57BL/6N	Tibialis anterior	Hiseq4000

Table2: List of the most dysregulated genes in MTM1-CNM mice.

Gene name	Log2FC Cohort MTM1-a	Log2FC Cohort MTM1-b	Log2FC Cohort MTM1-c	Log2FC Cohort MTM1-d
Sox11	6,16	4,70	5,80	3,97
Krt18	5,25	3,20	7,78	5,23
Gm28653	5,24	2,64	5,13	3,80
Mt3	4,76	3,31	5,28	4,66
Gm13583	4,65	3,17	6,53	8,15
Msln	4,61	3,28	3,96	4,19
Hsf2bp	4,32	3,48	4,24	4,21
Fosl1	4,21	2,69	4,81	6,85
C130080G10Rik	-1,88	-2,13	-3,36	-5,96
Amd1	-2,04	-2,66	-3,17	-2,72
Nt5c1a	-2,05	-2,54	-2,79	-3,77
Fam19a4	-2,31	-3,00	-2,55	-3,77
Ighm	-2,33	-2,89	-3,34	-2,55
Mtm1	-2,43	-2,12	-2,10	-2,55
Edn3	-2,51	-3,27	-2,93	-1,98
Cdh4	-2,57	-3,91	-3,63	-2,85
Mstn	-2,59	-1,79	-1,89	-2,72

Table3: RNA and protein levels of Mtm1 (MTM1), Bin1 (BIN1) and Dnm2 (DNM2) in *Mtm1*$^{-/y}$, *Bin1*$^{mck-/-}$, *Dnm2*$^{SL/+}$ and *Dnm2*$^{RW/+}$ mice.

Mouse line	RNA/Protein	MTM1	BIN1	DNM2
***Mtm1*$^{-/y}$**	Protein (WB)	Absent Age 5w (Cowling et al. 2014)	Fold = 2 P < 0.05 Age 7w (Lionello et al., 2019)	Fold = 2.5 P < 0.001 Age 5w (Cowling et al. 2014)
	RNA (qPCR)	Fold = 0.5 P = 0.0095 Age 7w	n.d.	Fold = 1.3 P < 0.05 Age 7w
	RNA (transcriptomic)	Fold = 0.2 P = 1.98E-09 Age 7w	Fold = 1.4 P = 0.046 Age 7w	Fold = 1.02 P = 0.95 Age 7w
***Bin1*$^{mck-/-}$**	Protein (WB)	Fold = 1.07 P= 0.95 Age 8w	Absent Unpublished	Fold = 1.5 P = 0.052 Age 8w Unpublished
	RNA (qPCR)	Fold = 0.97 P = 0.28 Age 7w	Absent P = 0.0091 Age 7w	Fold = 1.4 P < 0.05 Age 8w Unpublished
	RNA (transcriptomic)	Fold = 0.93 P= 0.63 Age 7w	Fold = 0.10 P = 1.63E-209 Age 7w	Fold = 1.1 P = 0.42 Age 7w
***Dnm2*$^{SL/+}$**	Protein (WB)	Fold = 0.7 Pval = 0.016 Age 8w	Fold = 0.95 Pval > 0.05 Age 8w	Fold = 2.2 Pval = 0.057 Age 8w
	RNA (qPCR)	Fold = P = 0.15 Age 7w	n.d.	Fold = P = 0.014 Age 7w
	RNA (transcriptomic)	Fold = 0.87 P = 0.023 Age 7w	Fold = 1.37 P= 2.34E-09 Age 7w	Fold = 1.04 P = 0.77 Age 7w

***Dnm2*$^{RW/+}$**	Prot	Fold = 1.2 P= 0.4 Age 7w	Fold = 1.8 P = 0.07 Age 7w	Fold = 1.05 P = 0.6 Age 7w

1140

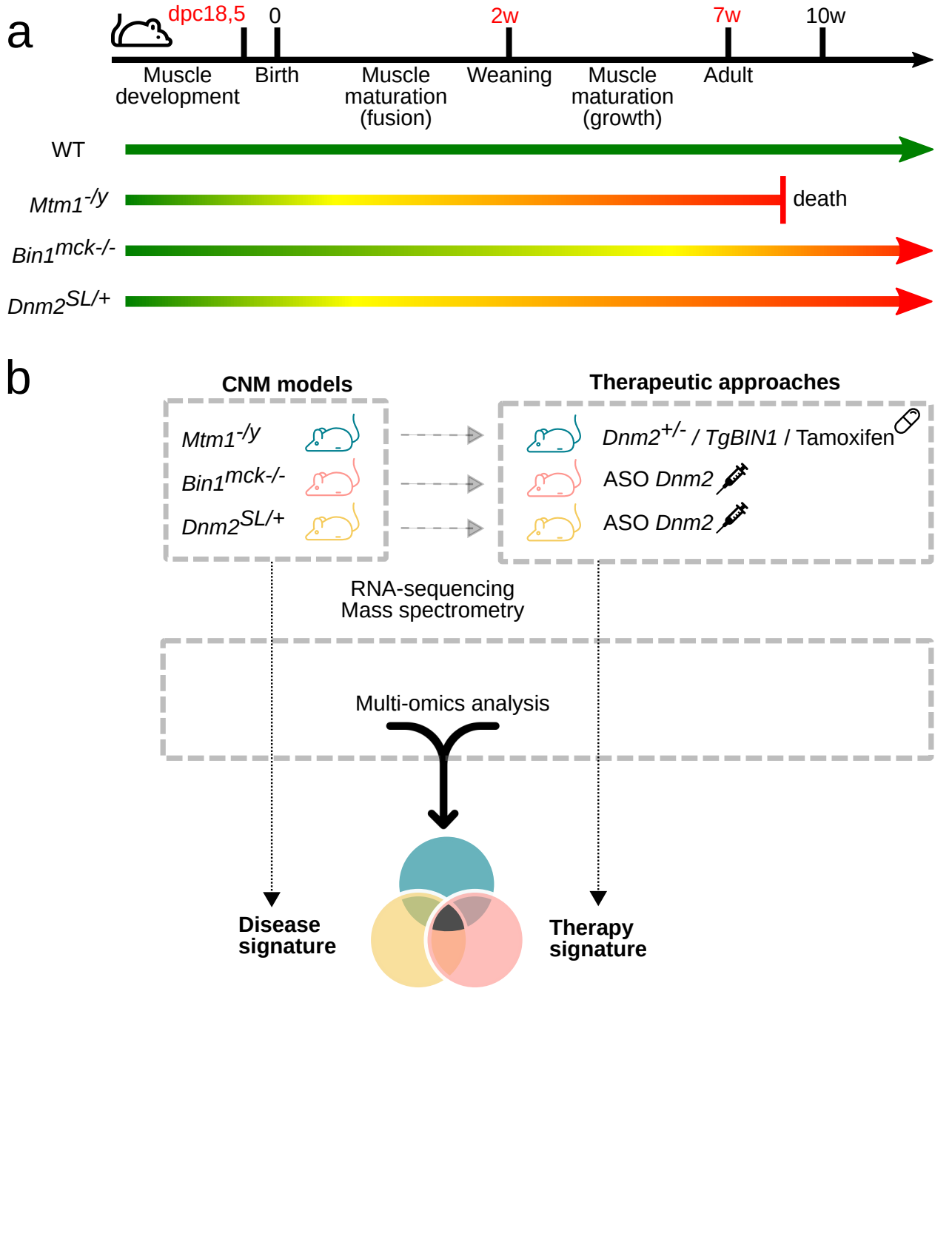
a
dpc18,5
0
2w
7w
10w
Muscle development
Birth
Muscle maturation (fusion)
Weaning
Muscle maturation (growth)
Adult
WT
Mtm1-/y
death
Bin1mck-/-
Dnm2SL/+
b
CNM models
Therapeutic approaches
Mtm1-/y
Bin1mck-/-
Dnm2SL/+
Dnm2+/- / TgBIN1 / Tamoxifen
ASO Dnm2
ASO Dnm2
RNA-sequencing
Mass spectrometry
Multi-omics analysis
Disease signature
Therapy signature

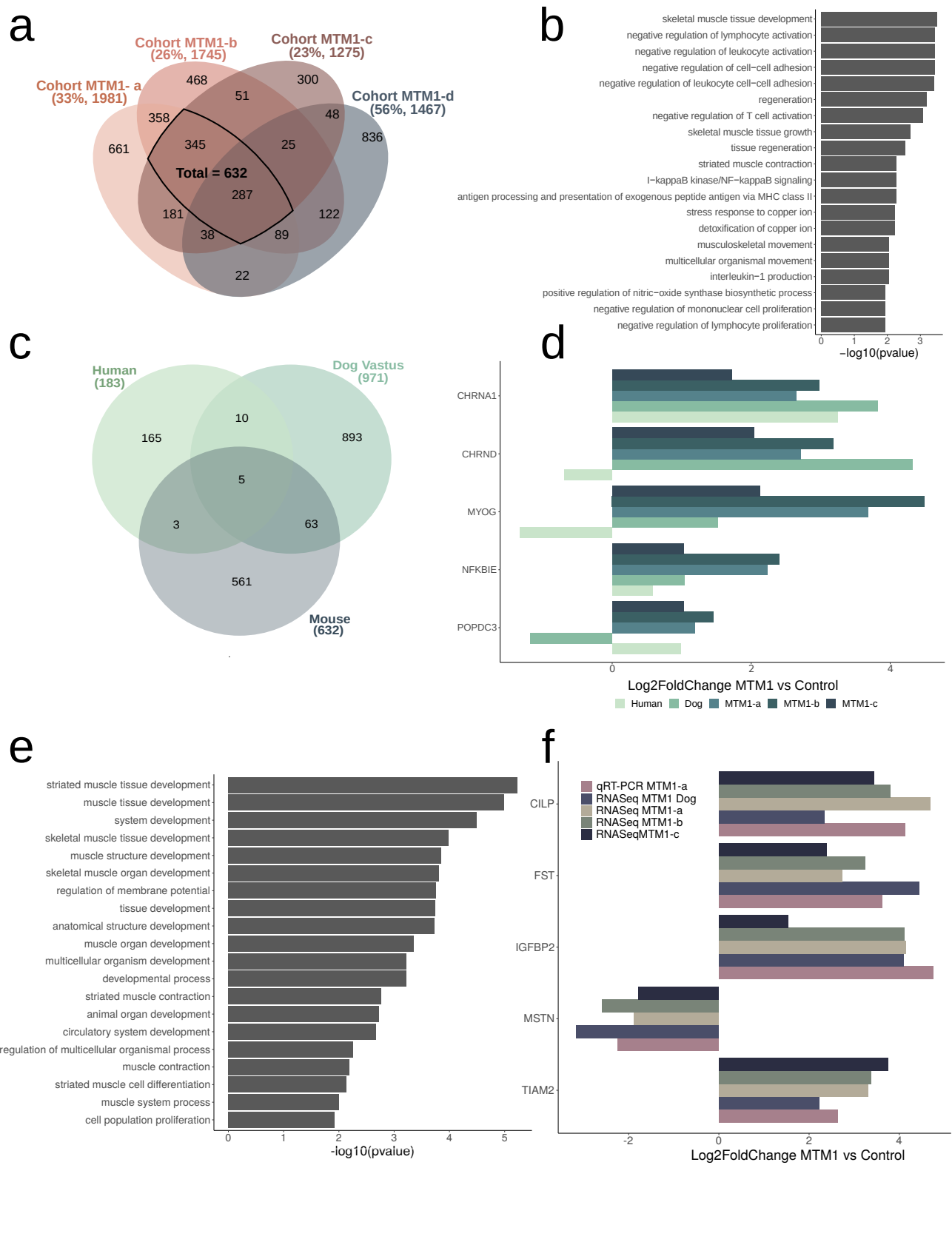
a
Cohort MTM1-b
(26%, 1745)
Cohort MTM1-c
(23%, 1275)
Cohort MTM1- a
(33%, 1981)
Cohort MTM1-d
(56%, 1467)
468
300
51
358
48
836
661
345
25
Total = 632
287
181
122
38
89
22
b
skeletal muscle tissue development
negative regulation of lymphocyte activation
negative regulation of leukocyte activation
negative regulation of cell−cell adhesion
negative regulation of leukocyte cell−cell adhesion
regeneration
negative regulation of T cell activation
skeletal muscle tissue growth
tissue regeneration
striated muscle contraction
I−kappaB kinase/NF−kappaB signaling
antigen processing and presentation of exogenous peptide antigen via MHC class II
stress response to copper ion
detoxification of copper ion
musculoskeletal movement
multicellular organismal movement
interleukin−1 production
positive regulation of nitric−oxide synthase biosynthetic process
negative regulation of mononuclear cell proliferation
negative regulation of lymphocyte proliferation
0
1
2
3
−log10(pvalue)
c
Human
(183)
Dog Vastus
(971)
10
165
893
5
3
63
561
Mouse
(632)
d
CHRNA1
CHRND
MYOG
NFKBIE
POPDC3
0
2
4
Log2FoldChange MTM1 vs Control
Human
Dog
MTM1-a
MTM1-b
MTM1-c
e
striated muscle tissue development
muscle tissue development
system development
skeletal muscle tissue development
muscle structure development
skeletal muscle organ development
regulation of membrane potential
tissue development
anatomical structure development
muscle organ development
multicellular organism development
developmental process
striated muscle contraction
animal organ development
circulatory system development
regulation of multicellular organismal process
muscle contraction
striated muscle cell differentiation
muscle system process
cell population proliferation
0
1
2
3
4
5
-log10(pvalue)
f
qRT-PCR MTM1-a
RNASeq MTM1 Dog
RNASeq MTM1-a
RNASeq MTM1-b
RNASeqMTM1-c
CILP
FST
IGFBP2
MSTN
TIAM2
-2
0
2
4
Log2FoldChange MTM1 vs Control

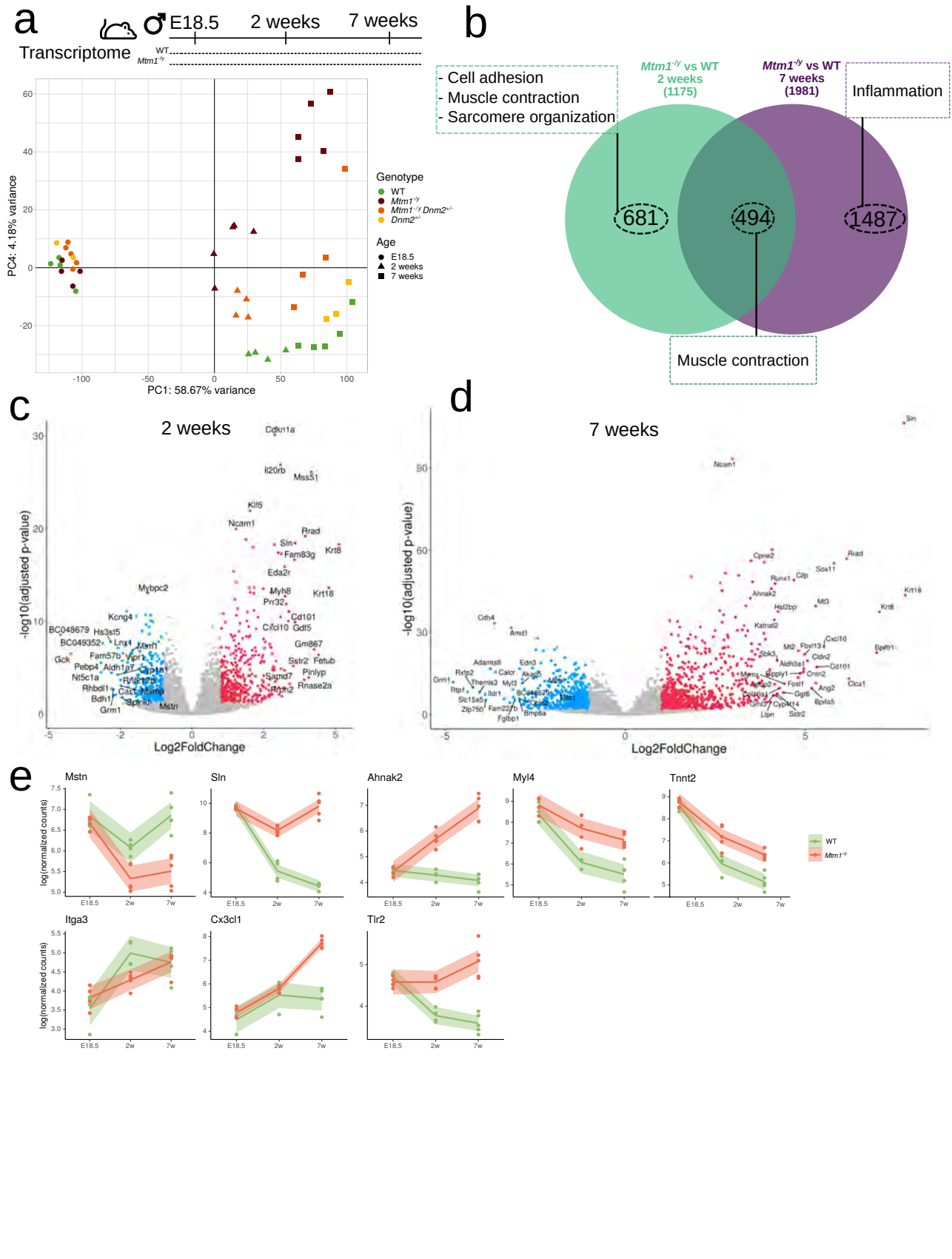
a
Transcriptome
♂
E18.5
2 weeks
7 weeks
WT
Mtm1-/y
PC4: 4.18% variance
PC1: 58.67% variance
Genotype
WT
Mtm1-/y
Mtm1-/y Dnm2+/-
Dnm2+/-
Age
E18.5
2 weeks
7 weeks
b
- Cell adhesion
- Muscle contraction
- Sarcomere organization
Mtm1-/y vs WT
2 weeks
(1175)
Mtm1-/y vs WT
7 weeks
(1981)
Inflammation
681
494
1487
Muscle contraction
c
2 weeks
-log10(adjusted p-value)
Log2FoldChange
d
7 weeks
-log10(adjusted p-value)
Log2FoldChange
e
Mstn
Sln
Ahnak2
Myl4
Tnnt2
Itga3
Cx3cl1
Tlr2
log(normalized counts)
E18.5
2w
7w
WT
Mtm1-/y

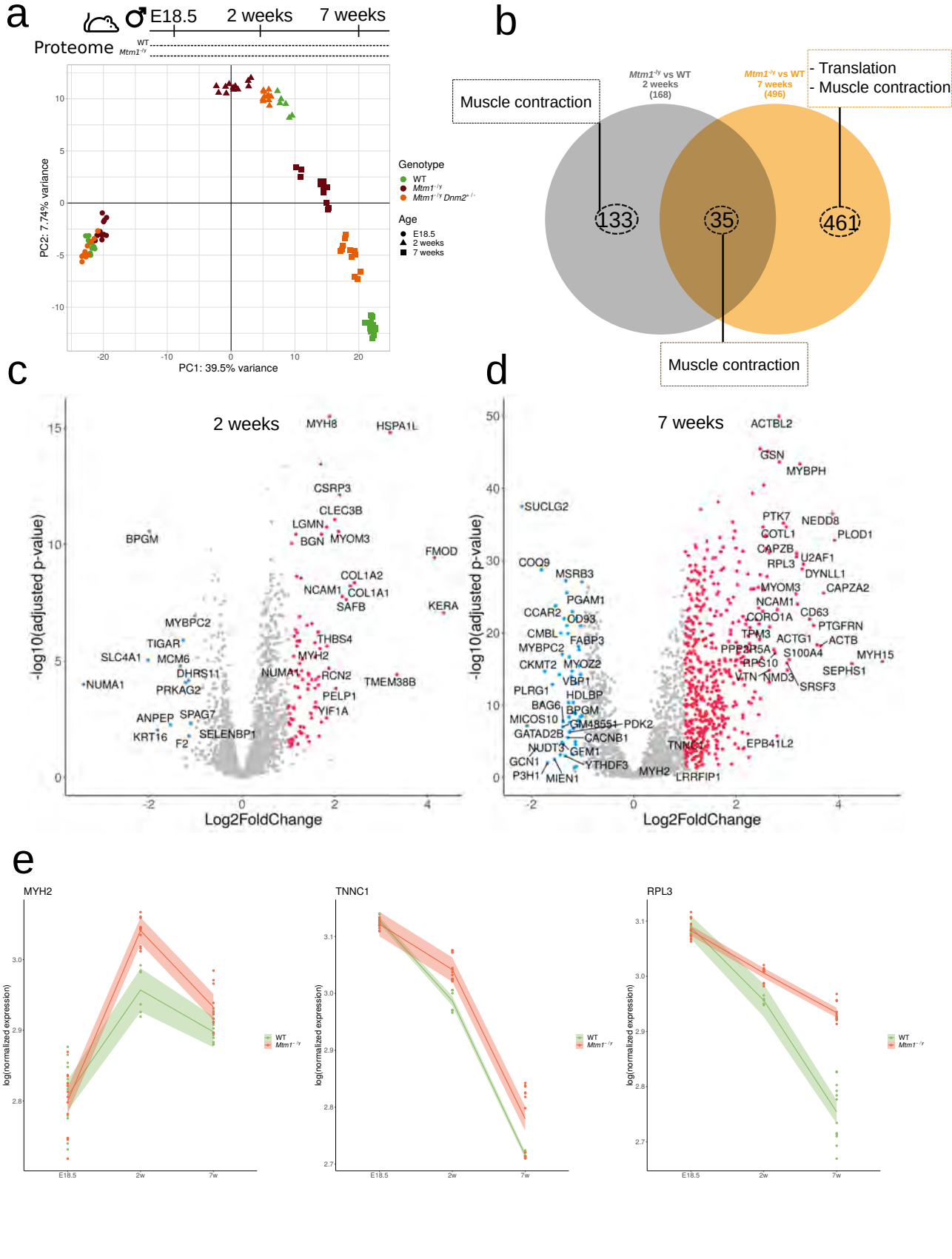
a
E18.5
2 weeks
7 weeks
Proteome
WT
Mtm1-/y
PC2: 7.74% variance
PC1: 39.5% variance
Genotype
WT
Mtm1-/y
Mtm1-/y Dnm2+/-
Age
E18.5
2 weeks
7 weeks
b
Mtm1-/y vs WT
2 weeks
(168)
Mtm1-/y vs WT
7 weeks
(496)
Muscle contraction
- Translation
- Muscle contraction
133
35
461
Muscle contraction
c
2 weeks
-log10(adjusted p-value)
Log2FoldChange
MYH8
HSPA1L
CSRP3
CLEC3B
LGMN
BGN
MYOM3
BPGM
FMOD
COL1A2
NCAM1
COL1A1
SAFB
KERA
MYBPC2
TIGAR
THBS4
SLC4A1
MCM6
MYH2
DHRS11
NUMA1
RCN2
TMEM38B
NUMA1
PRKAG2
PELP1
YIF1A
ANPEP
SPAG7
KRT16
F2
SELENBP1
d
7 weeks
-log10(adjusted p-value)
Log2FoldChange
ACTBL2
GSN
MYBPH
SUCLG2
PTK7
NEDD8
GOTL1
PLOD1
CAPZB
U2AF1
RPL3
DYNLL1
COQ9
MSRB3
MYOM3
CAPZA2
PGAM1
NCAM1
CCAR2
CD93
CORO1A
CD63
CMBL
FABP3
TPM3
ACTG1
PTGFRN
ACTB
MYBPC2
PPP2R5A
S100A4
MYH15
CKMT2
MYOZ2
RPS10
SEPHS1
VBP1
VTN
NMD3
PLRG1
HDLBP
SRSF3
BAG6
BPGM
MICOS10
GM48551
PDK2
GATAD2B
CACNB1
EPB41L2
NUDT3
GEM1
TNNC1
GCN1
YTHDF3
P3H1
MIEN1
MYH2
LRRFIP1
e
MYH2
TNNC1
RPL3
log(normalized expression)
WT
Mtm1-/y
E18.5
2w
7w

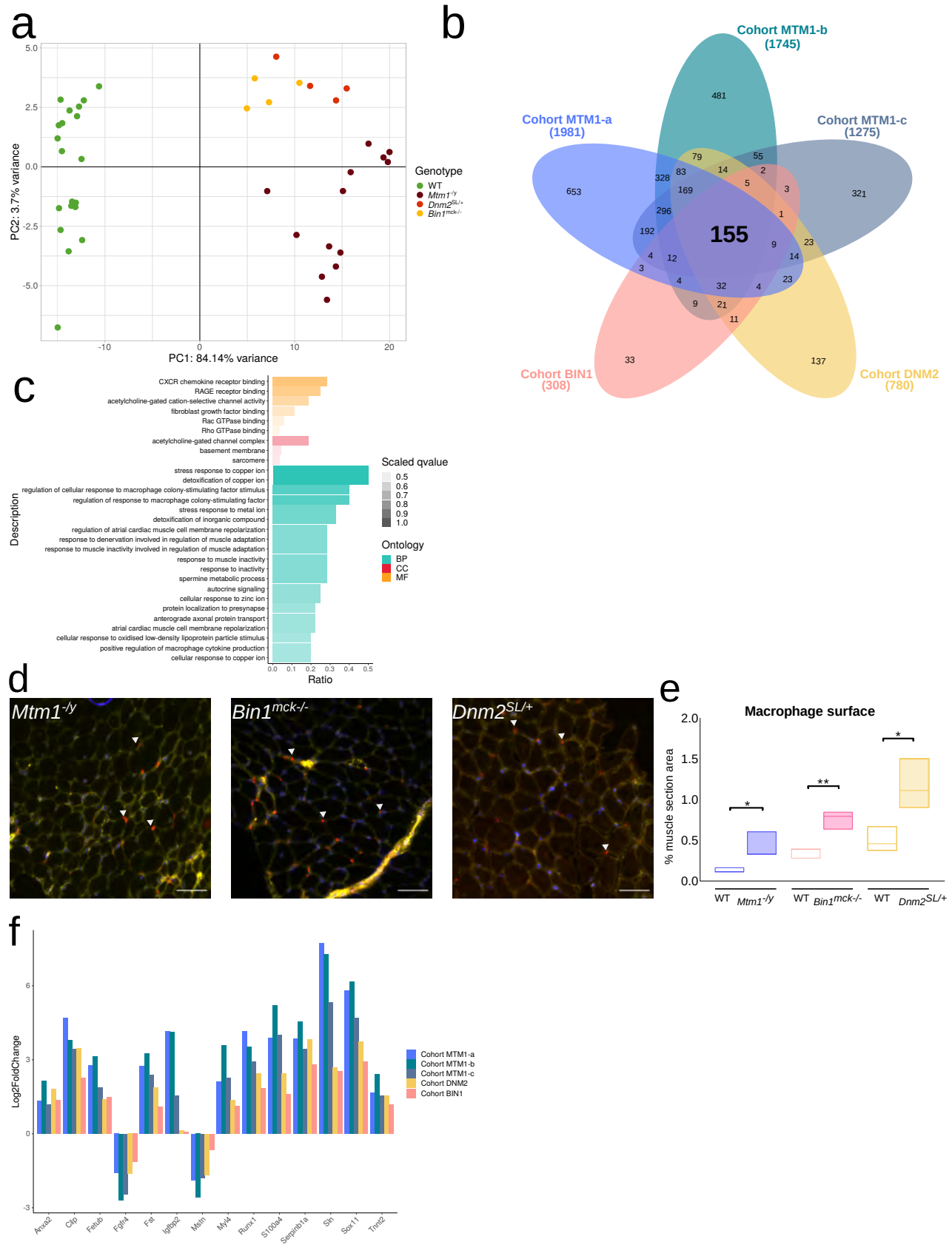
a
PC2: 3.7% variance
PC1: 84.14% variance
Genotype
WT
Mtm1-/y
Dnm2SL/+
Bin1mck-/-
b
Cohort MTM1-b (1745)
Cohort MTM1-a (1981)
Cohort MTM1-c (1275)
Cohort BIN1 (308)
Cohort DNM2 (780)
155
c
Description
Ratio
Scaled qvalue
Ontology
BP
CC
MF
CXCR chemokine receptor binding
RAGE receptor binding
acetylcholine-gated cation-selective channel activity
fibroblast growth factor binding
Rac GTPase binding
Rho GTPase binding
acetylcholine-gated channel complex
basement membrane
sarcomere
stress response to copper ion
detoxification of copper ion
regulation of cellular response to macrophage colony-stimulating factor stimulus
regulation of response to macrophage colony-stimulating factor
stress response to metal ion
detoxification of inorganic compound
regulation of atrial cardiac muscle cell membrane repolarization
response to denervation involved in regulation of muscle adaptation
response to muscle inactivity involved in regulation of muscle adaptation
response to muscle inactivity
response to inactivity
spermine metabolic process
autocrine signaling
cellular response to zinc ion
protein localization to presynapse
anterograde axonal protein transport
atrial cardiac muscle cell membrane repolarization
cellular response to oxidised low-density lipoprotein particle stimulus
positive regulation of macrophage cytokine production
cellular response to copper ion
d
Mtm1-/y
Bin1mck-/-
Dnm2SL/+
e
Macrophage surface
% muscle section area
WT
Mtm1-/y
Bin1mck-/-
Dnm2SL/+
f
Log2FoldChange
Cohort MTM1-a
Cohort MTM1-b
Cohort MTM1-c
Cohort DNM2
Cohort BIN1
Anxa2
Clip
Fetub
Fgfr4
Fst
Igfbp2
Msln
Myl4
Runx1
S100a4
Serpinb1a
Sln
Sox11
Tnnt2

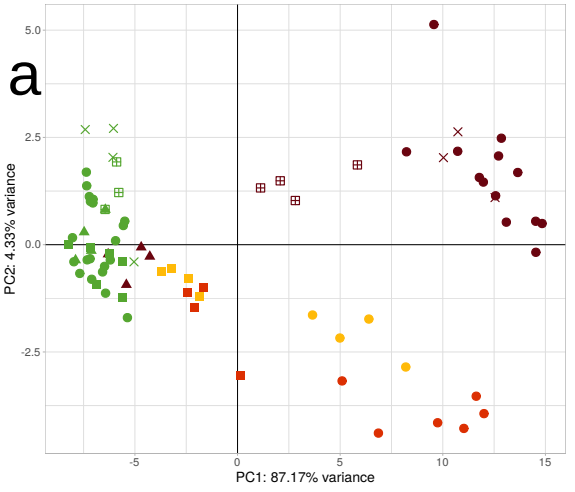

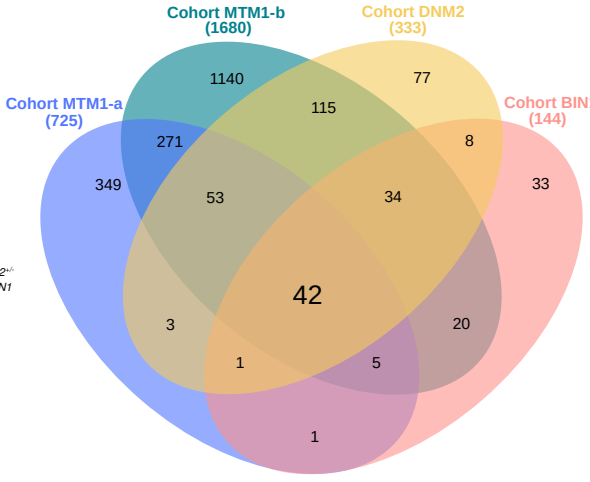

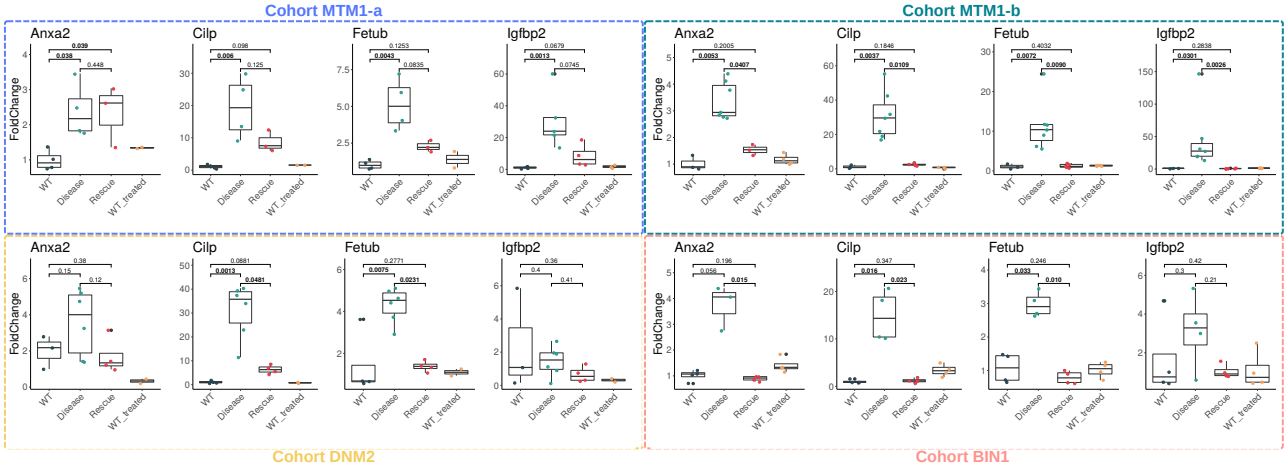

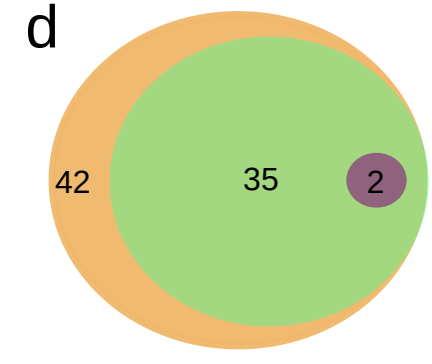

42 genes common to therapies
AND
35 human orthologs
AND
2 targeted by drug

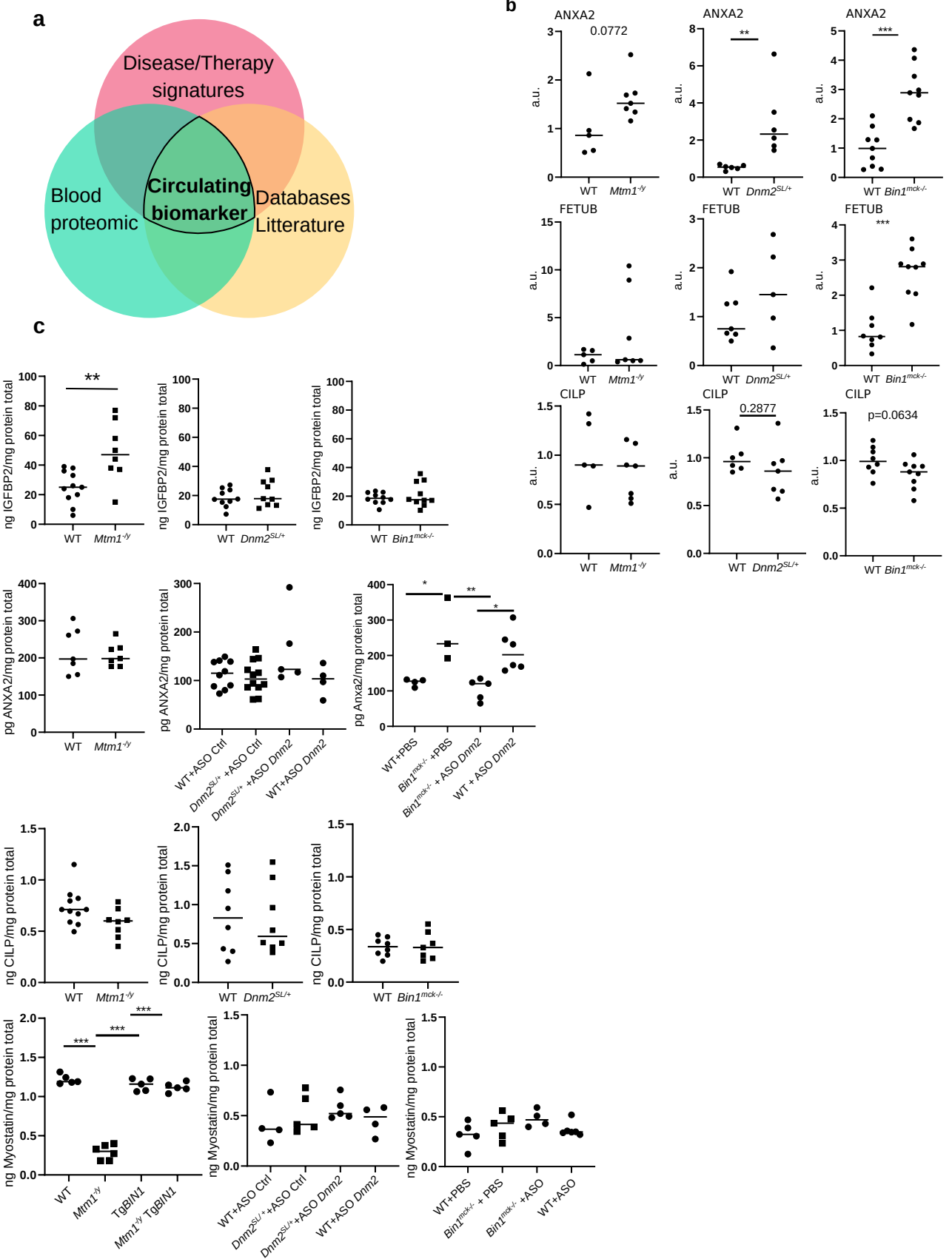
a
Disease/Therapy signatures
Blood proteomic
Circulating biomarker
Databases Litterature
b
ANXA2
0.0772
**
***
FETUB
***
CILP
0.2877
p=0.0634
a.u.
WT
Mtm1-/-
Dnm2SL/+
Bin1mck-/-
c
ng IGFBP2/mg protein total
pg ANXA2/mg protein total
pg Anxa2/mg protein total
ng CILP/mg protein total
ng Myostatin/mg protein total
WT+ASO Ctrl
Dnm2SL/+ +ASO Ctrl
Dnm2SL/+ +ASO Dnm2
WT+ASO Dnm2
WT+PBS
Bin1mck-/- +PBS
Bin1mck-/- + ASO Dnm2
WT + ASO Dnm2
TgBIN1
Mtm1-/- TgBIN1
Bin1mck-/- + PBS
Bin1mck-/- +ASO
WT+ASO

Supplementary Figures S1

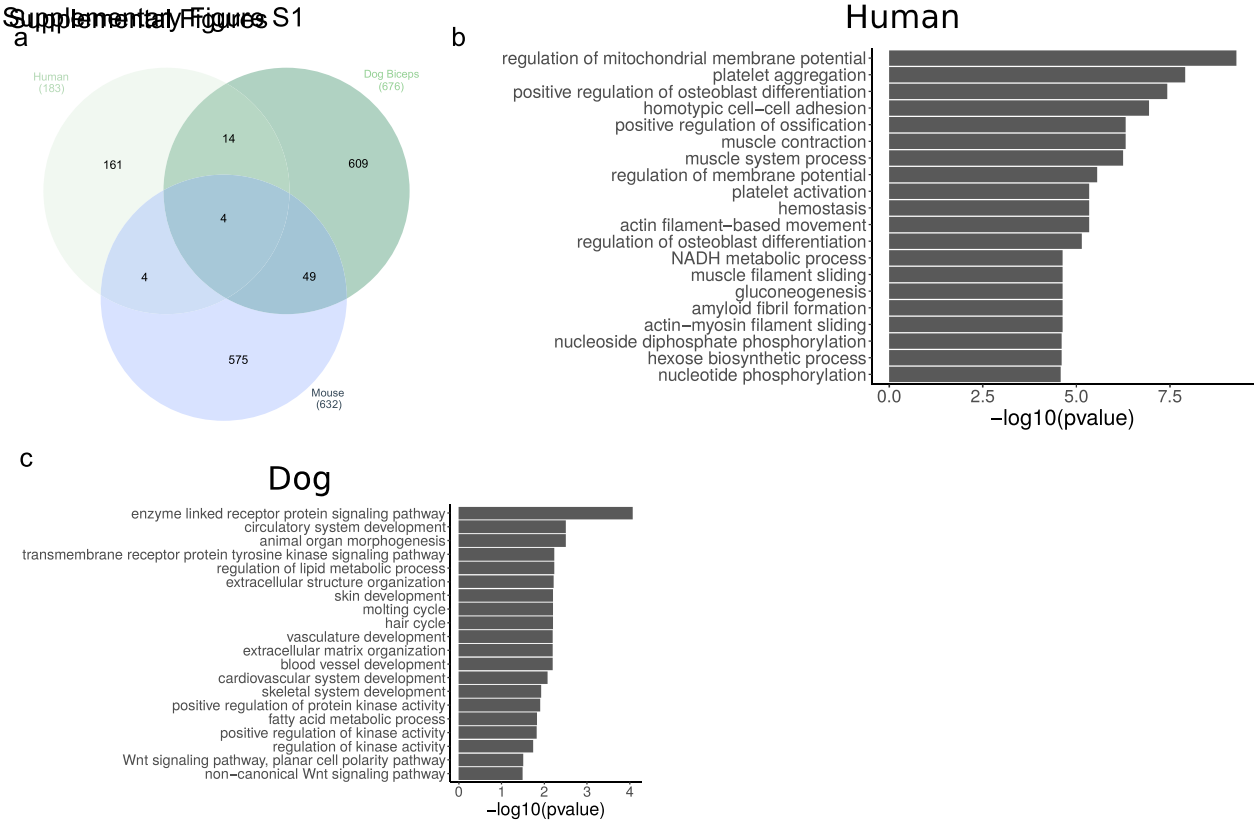

Supplementary Figure S2

a

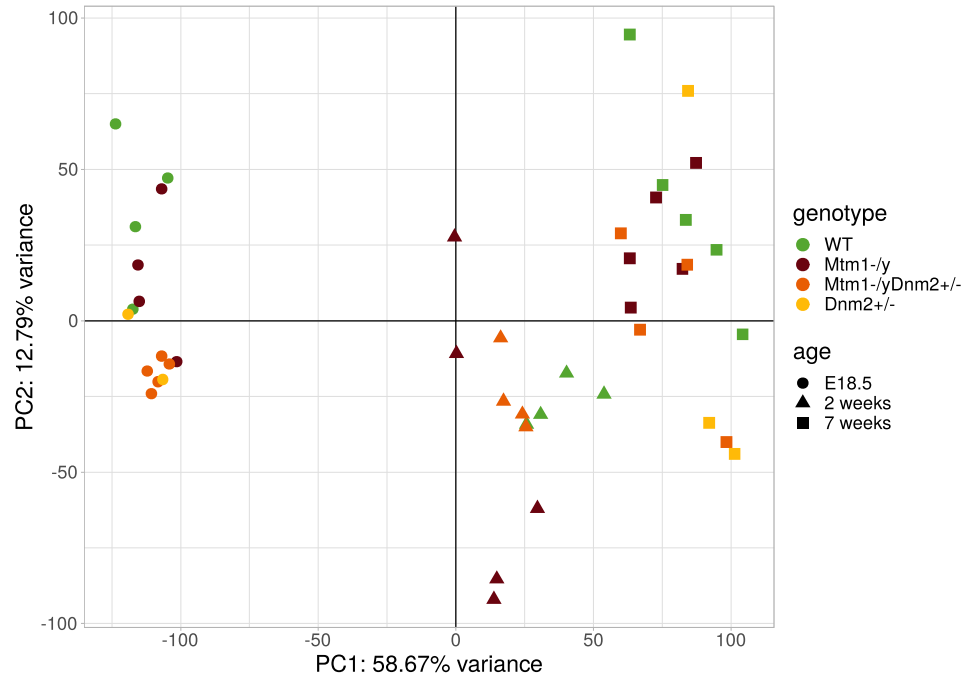

b

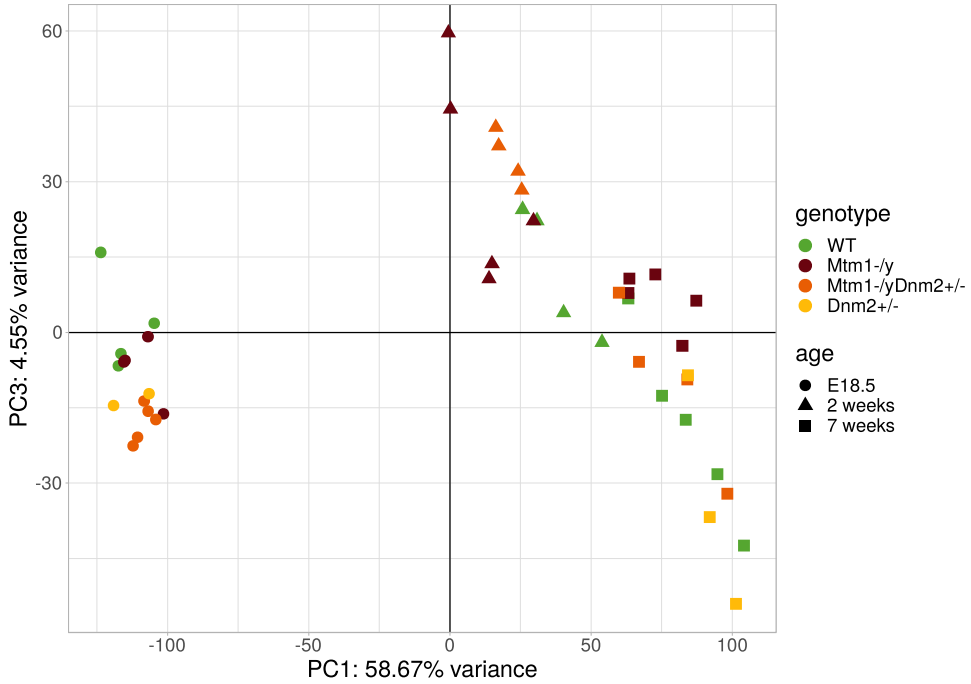

Supplementary Figure S3

Supplementary Figure S4

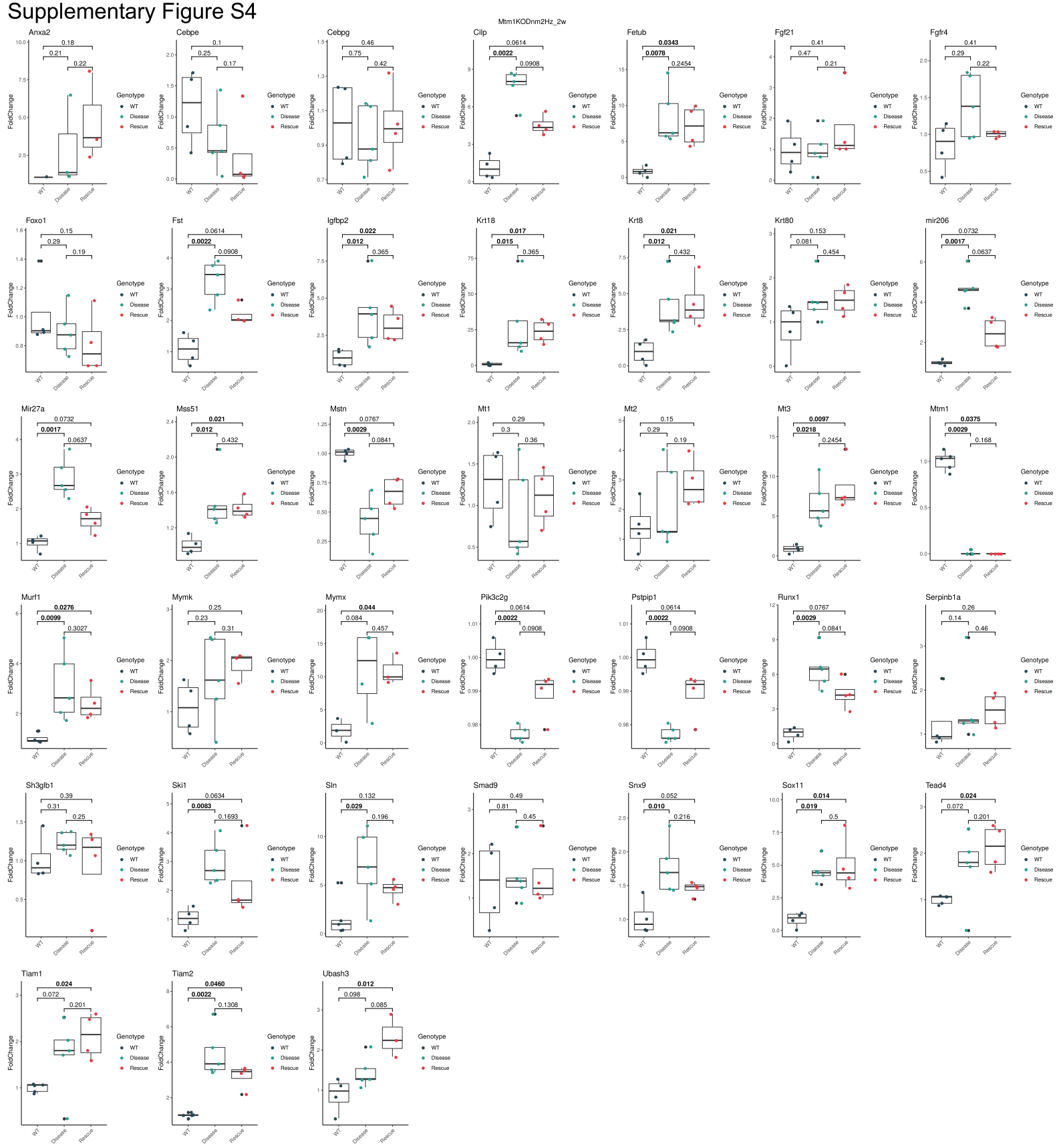

Supplementary Figure S5

Supplementary Figure S6

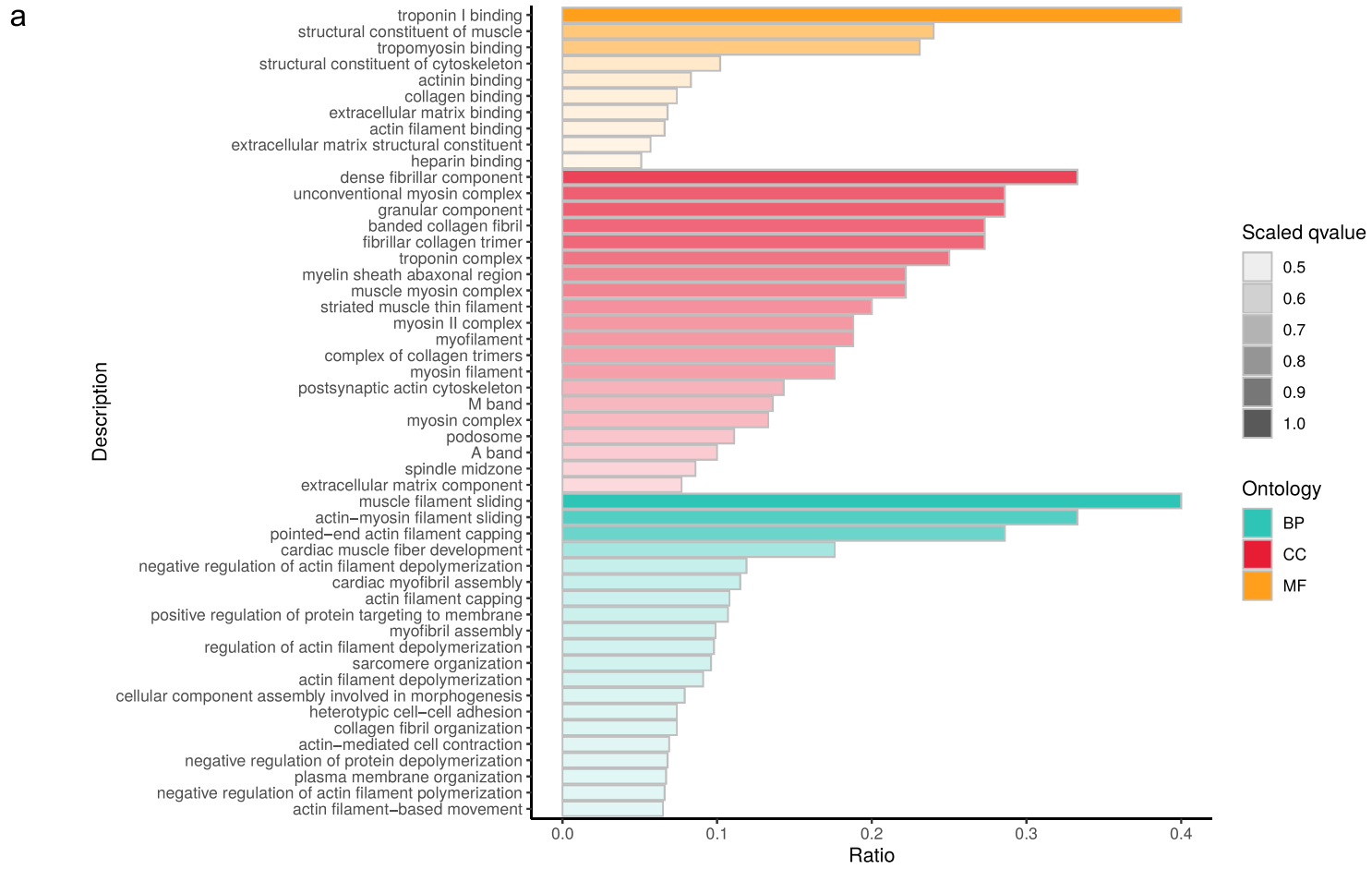

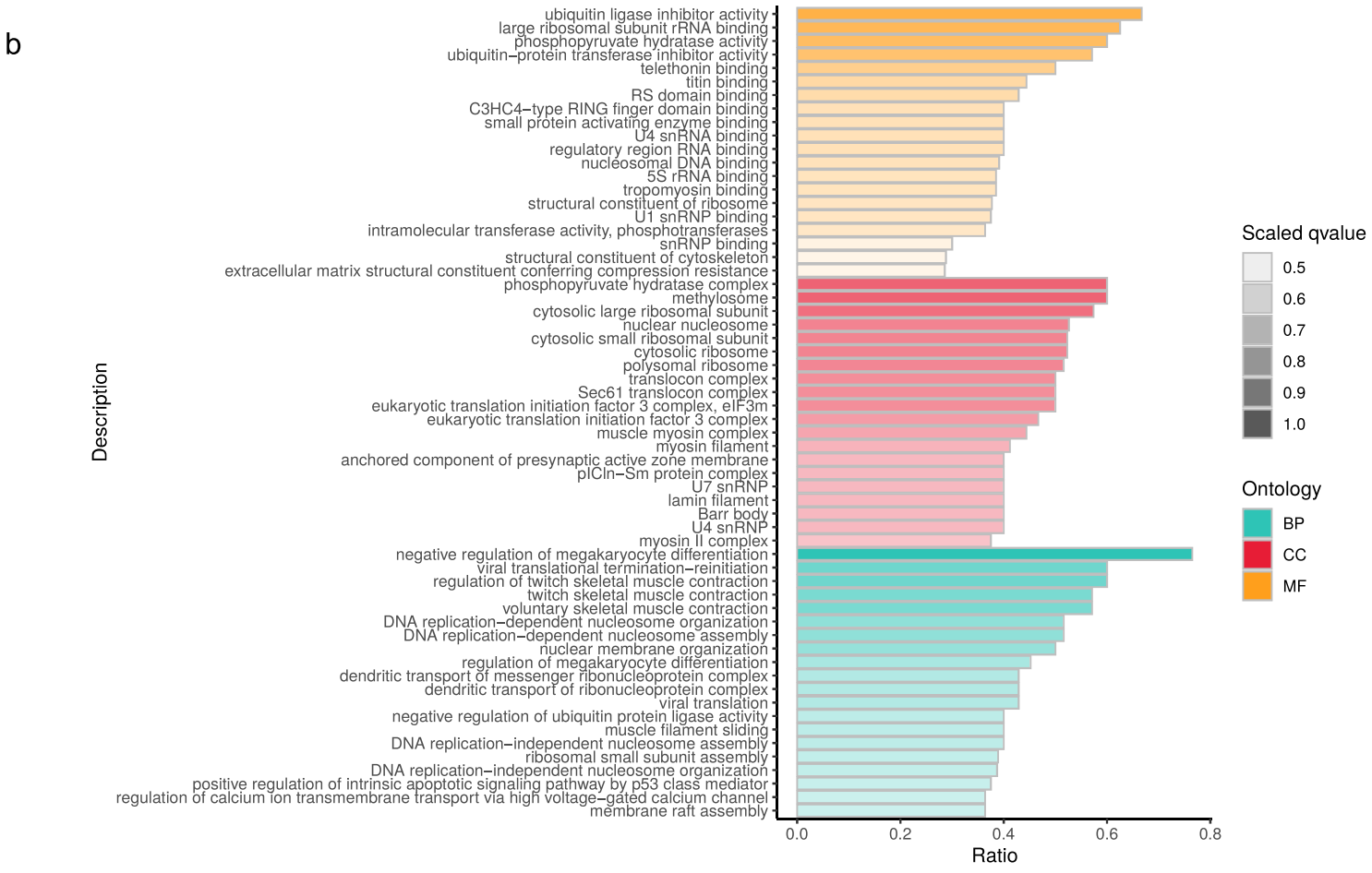

Supplementary Figure S7

a

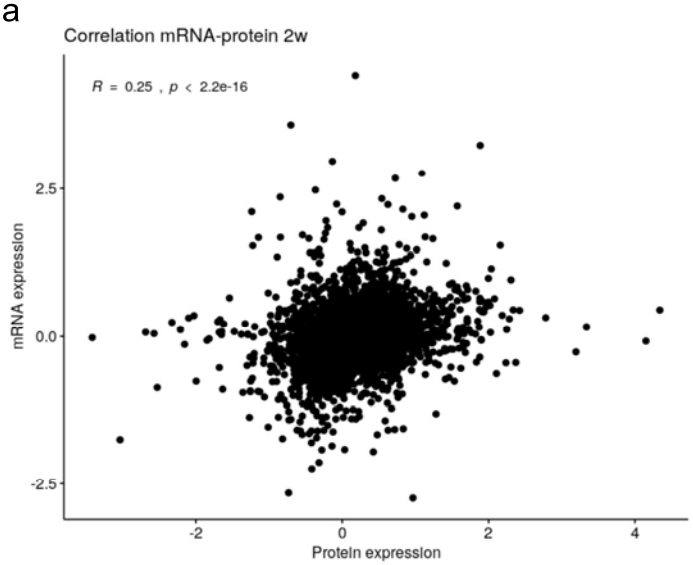

b

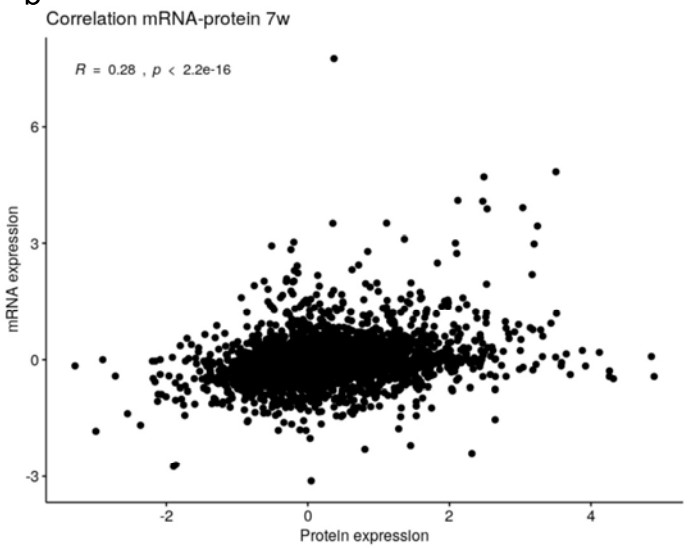

Supplementary Figure S8

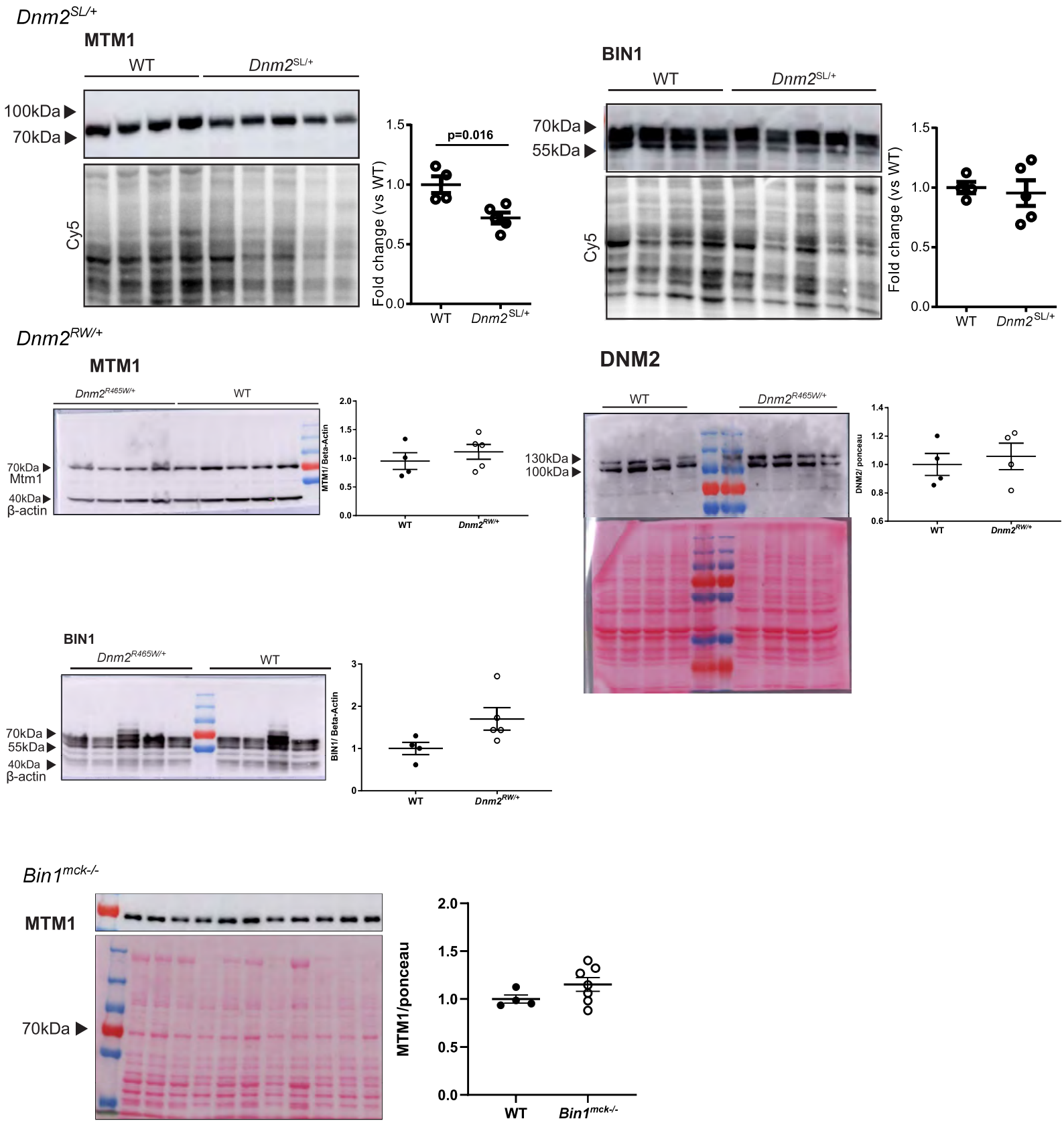

Supplementary Figure S9

a

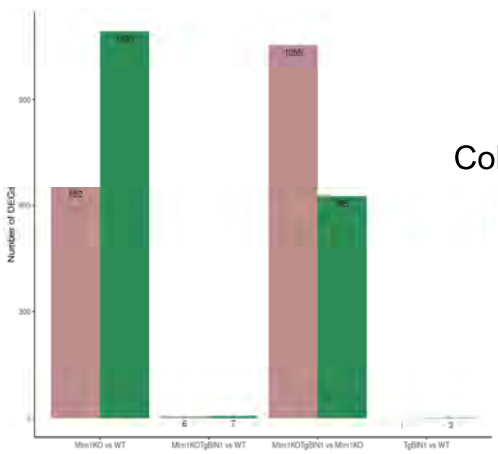

Cohort MTM1-b

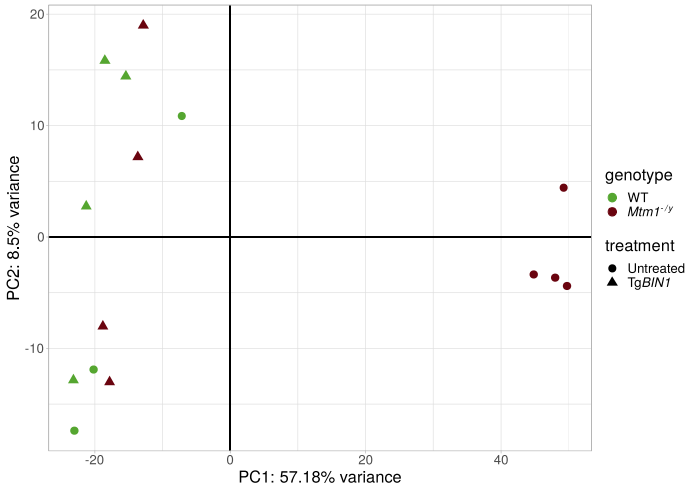

b

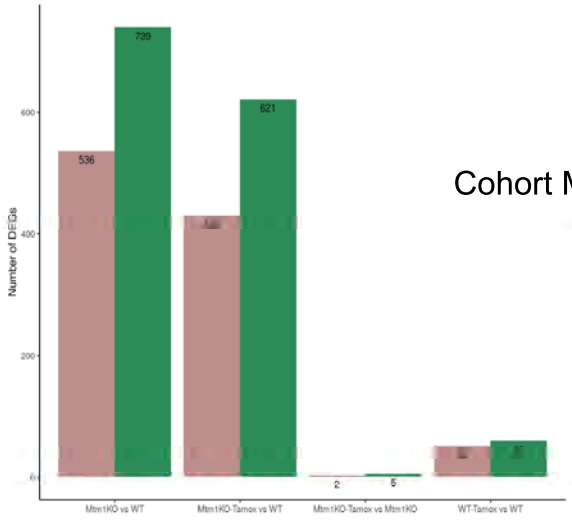

Cohort MTM1-c

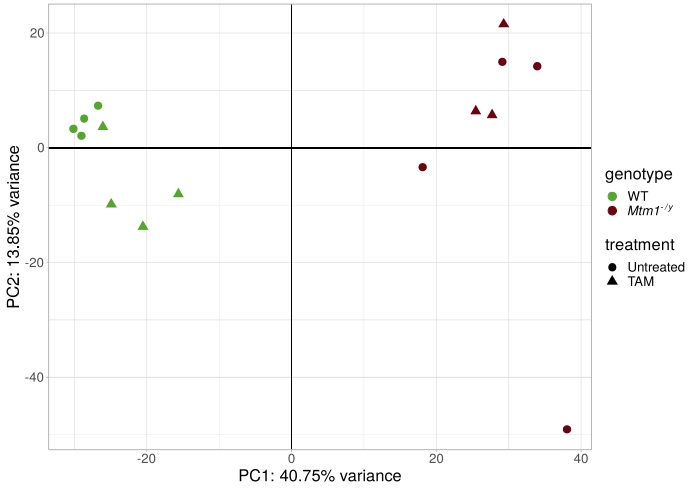

c

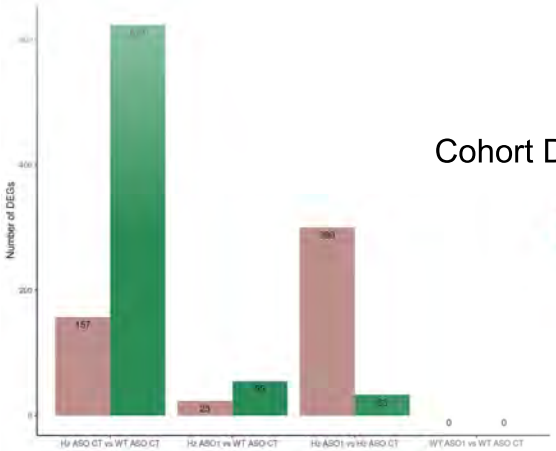

Cohort DNM2

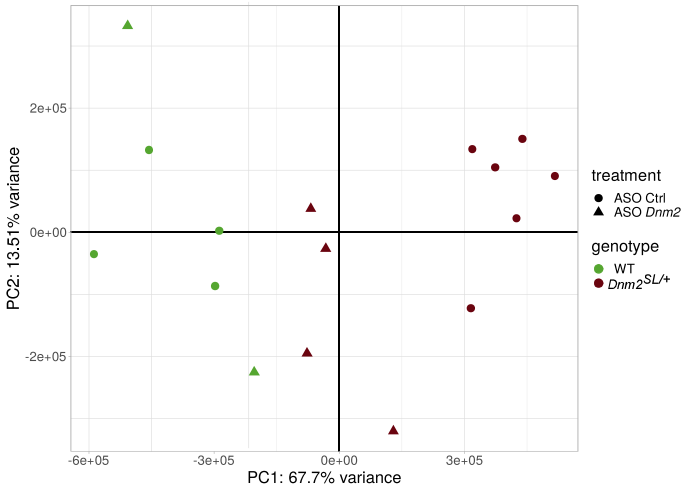

d

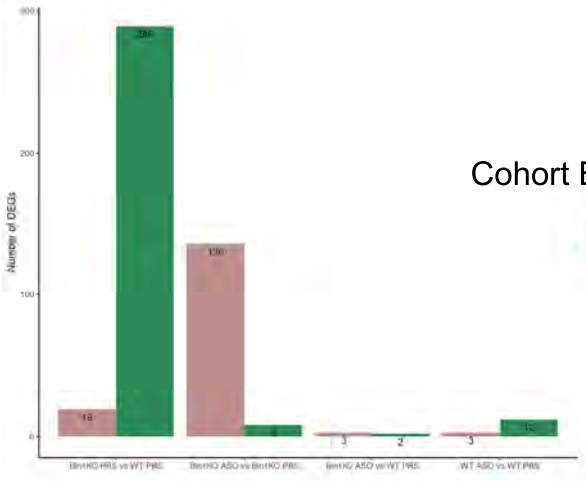

Cohort BIN1

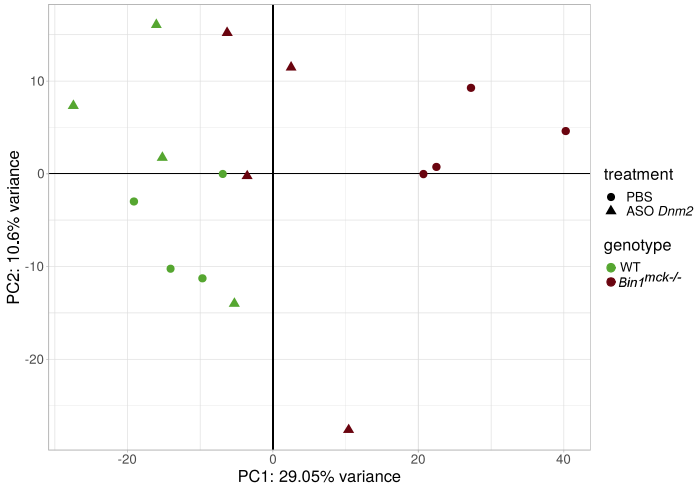

Supplementary Figure S10

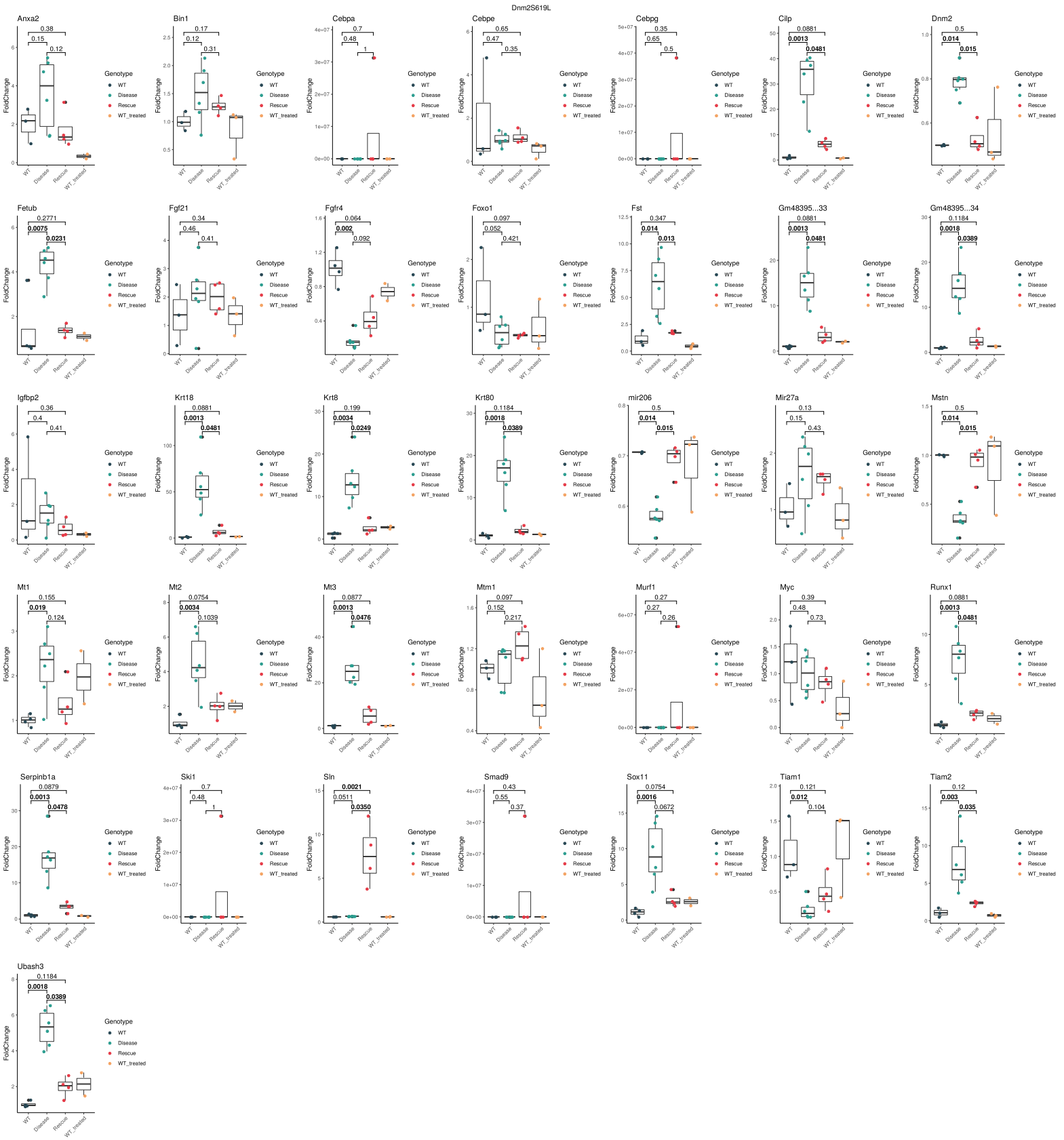

Supplementary Figure S11

Supplementary Figure S12

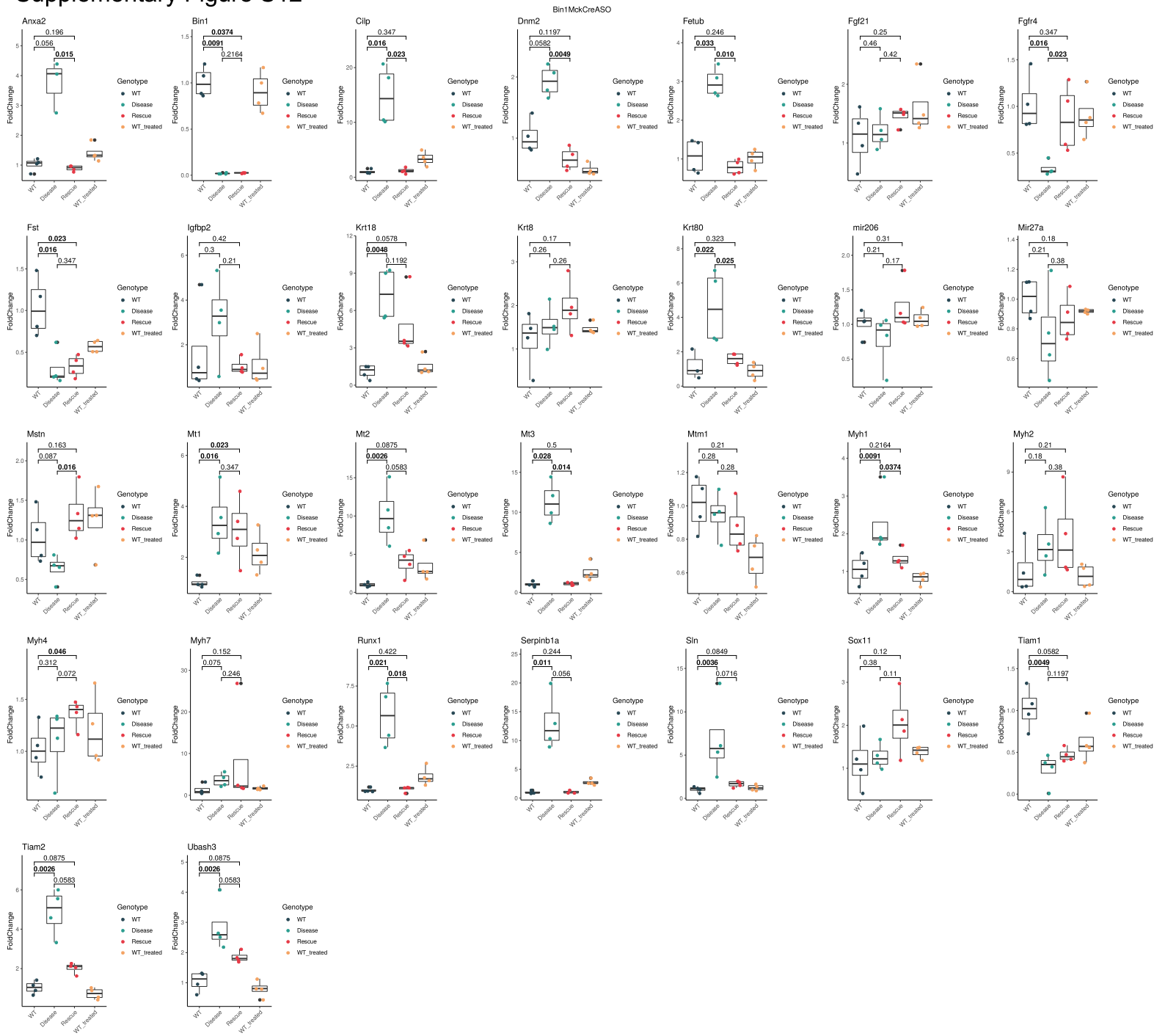

Supplementary Figure S13

a Cohort MTM1

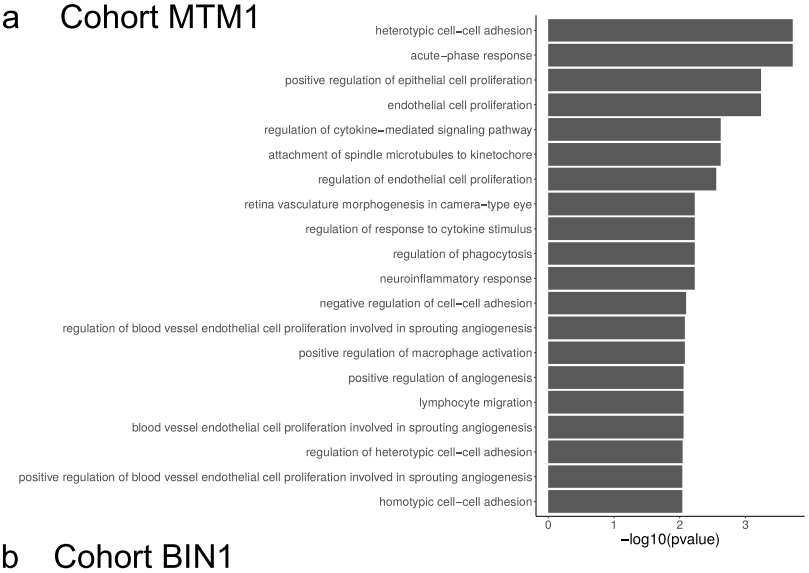

b Cohort BIN1

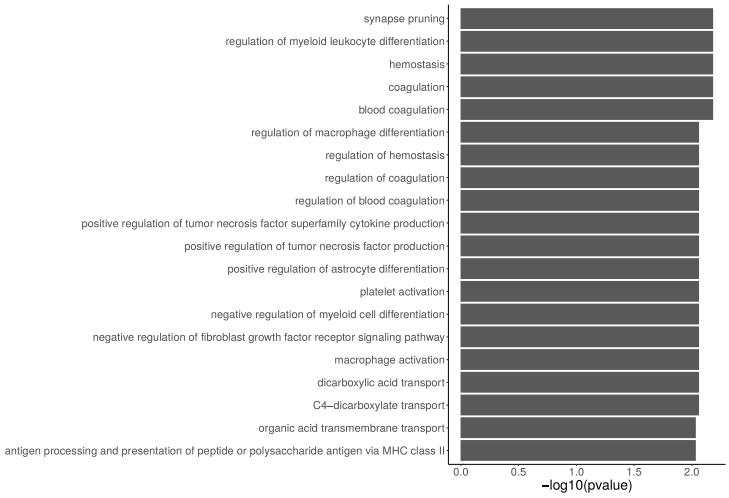

c Cohort DNM2

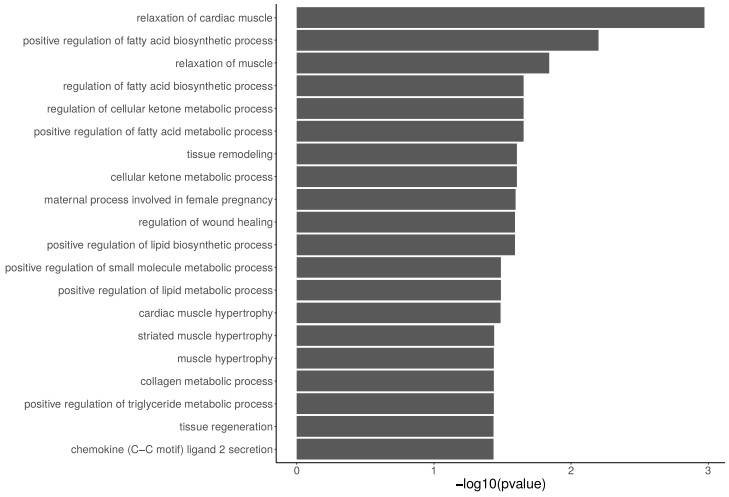

Supplementary Figure S14

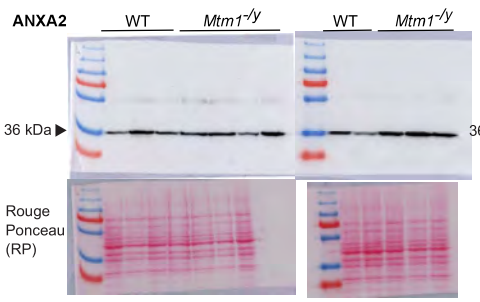

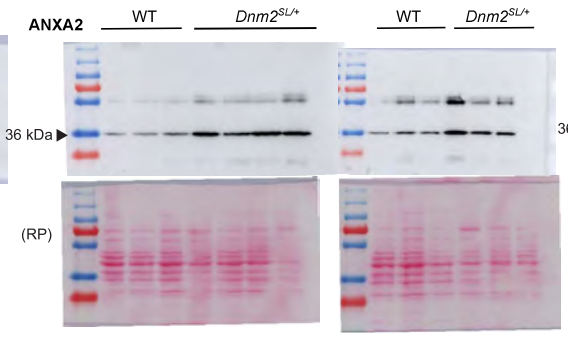

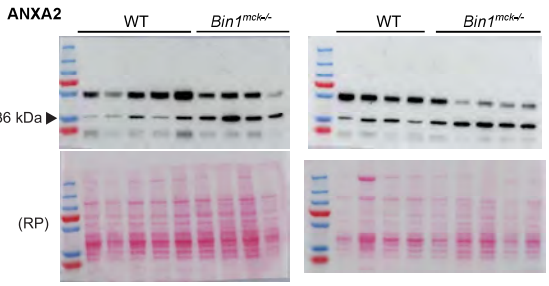

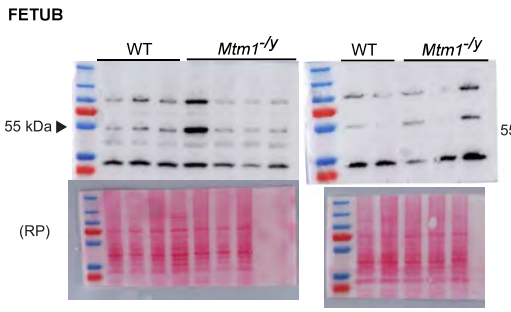

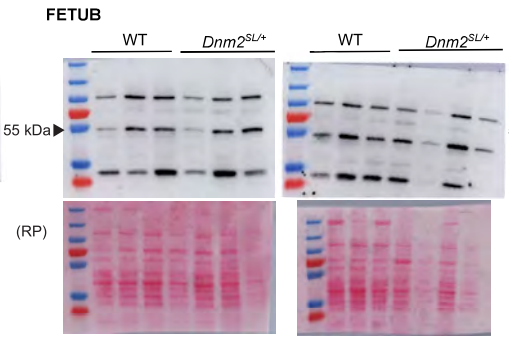

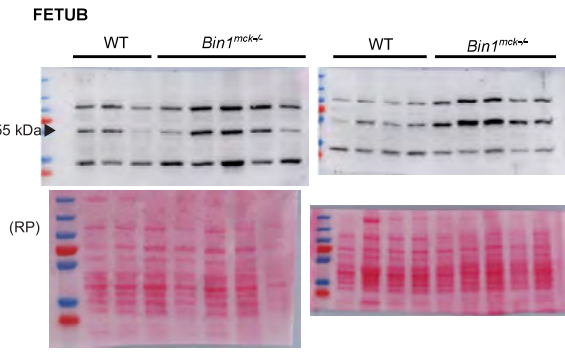

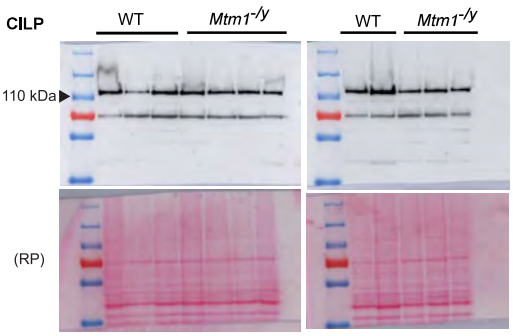

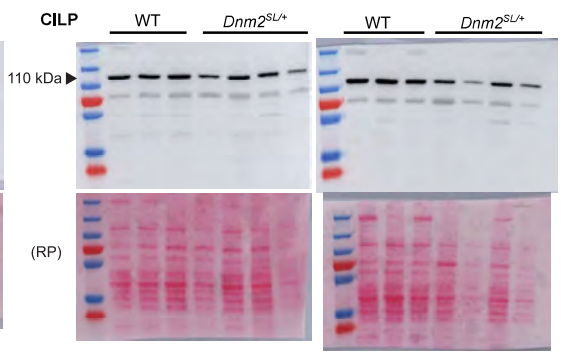

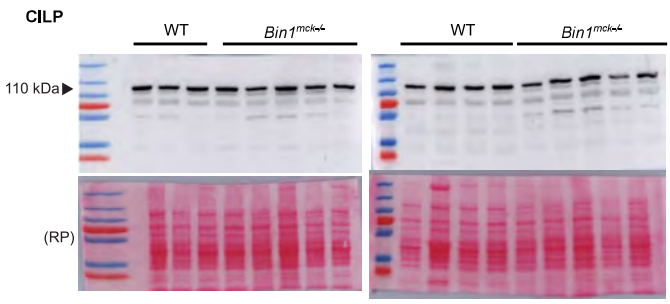

Supplementary Figure S15